



Review

# Monitoring Heavy Metals and Metalloids in Soils and Vegetation by Remote Sensing: A Review

Viktoriia Lovynska <sup>1,2</sup>, Bagher Bayat <sup>1</sup>, Roland Bol <sup>1</sup>, Shirin Moradi <sup>1</sup>, Mehdi Rahmati <sup>1</sup>, Rahul Raj <sup>1</sup>, Svitlana Sytnyk <sup>2,3</sup>, Oliver Wiche <sup>4</sup>, Bei Wu <sup>1</sup>, and Carsten Montzka <sup>1,\*</sup>

- Institute of Bio- and Geosciences: Agrosphere (IBG-3), Forschungszentrum Jülich, 52425 Jülich, Germany; v.lovynska@fz-juelich.de (V.L.); b.bayat@fz-juelich.de (B.B.); r.bol@fz-juelich.de (R.B.); s.moradi@fz-juelich.de (S.M.); m.rahmati@fz-juelich.de (M.R.); r.raj@fz-juelich.de (R.R.); b.wu@fz-juelich.de (B.W.)
- <sup>2</sup> Laboratory of Forestry, Dnipro State Agrarian and Economic University, 49009 Dnipro, Ukraine; svitlana.sytnyk@uni-bielefeld.de
- <sup>3</sup> Chemical Ecology Group, Bielefeld University, 33615 Bielefeld, Germany
- <sup>4</sup> Applied Geoecology Group, Faculty of Natural and Environmental Sciences, Zittau/Görlitz University of Applied Sciences, 02763 Zittau, Germany; oliver.wiche@hszg.de
- \* Correspondence: c.montzka@fz-juelich.de; Tel.: +49-2461-613289

Abstract: Heavy metal contamination in soils and vegetation poses a significant problem due to its toxicity and persistence. Toxic effects on vegetation include not only impaired growth, reduced yields, and even plant death but also biodiversity loss and ecosystem degradation. Addressing this issue requires comprehensive monitoring and remediation efforts to mitigate the environmental, human health, and ecological impacts. This review examines the state-of-the-art methodologies and advancements in remote sensing applications for detecting and monitoring heavy metal contamination in soil and its subsequent effects on vegetation. By synthesizing the current research findings and technological developments, this review offers insights into the efficacy and potential of remote sensing for monitoring heavy metal contamination in terrestrial ecosystems. However, current studies focus on regression and AI methods to link spectral reflectances and indices to heavy metal concentrations, which poses limited transferability to other areas, times, spectral discretizations, and heavy metal elements. We conclude that one important way forward is the more thorough understanding and simulation of the related physico-chemical processes in soils and plants and their effects on the spectral signatures. This would offer a profound basis for remote sensing applications for individual circumstances and would allow disentangling heavy metal effects from other stressors such as droughts or soil salinity.

Keywords: heavy metal; metalloids; pollution; remote sensing



Citation: Lovynska, V.; Bayat, B.; Bol, R.; Moradi, S.; Rahmati, M.; Raj, R.; Sytnyk, S.; Wiche, O.; Wu, B.; Montzka, C. Monitoring Heavy Metals and Metalloids in Soils and Vegetation by Remote Sensing:

A Review. *Remote Sens.* 2024, 16, 3221. https://doi.org/10.3390/rs16173221

Academic Editor: Eyal Ben-Dor

Received: 3 July 2024 Revised: 22 August 2024 Accepted: 23 August 2024 Published: 30 August 2024



Copyright: © 2024 by the authors. Licensee MDPI, Basel, Switzerland. This article is an open access article distributed under the terms and conditions of the Creative Commons Attribution (CC BY) license (https://creativecommons.org/licenses/by/4.0/).

# 1. Introduction

Heavy metal (HM) and metalloid pollution is a significant environmental concern resulting from the release of metallic elements into the environment, presenting substantial threats to ecosystems and human well-being. The term "heavy metal" refers to metallic elements and metalloids with a density surpassing 5000 kg·m<sup>-3</sup> and an atomic mass exceeding 20 [1]. Though HMs have a persistent nature and do not break down, they can be leached, dissolved, and/or transformed, in many cases into more toxic forms, and accumulate in the environment and living beings. Even in minor quantities, HMs can induce harmful effects on living organisms, disrupting biological processes and setting off a chain reaction of ecological imbalances. Their enduring presence in the environment exacerbates this issue, as they have the propensity to bioaccumulate in the food chain, posing risks to both wildlife and human populations [2]. A critical understanding of the sources, pathways, and impacts of HM pollution becomes imperative for formulating

Remote Sens. 2024, 16, 3221 2 of 30

effective strategies to mitigate its consequences and safeguard the well-being of ecosystems and human societies.

HM pollution arises from diverse origins, encompassing a range of natural processes and human-induced activities [3]. They are relatively scarcely present in the earth's crust and are naturally released into the environment from rocks and minerals by geological processes, such as weathering and erosion, influencing soil composition and water quality in ways that have occurred over geological time scales. Industrial activities, especially those associated with mining and metallurgy, release significant quantities of HMs into the environment [4]. The inadequate disposal of electronic waste, industrial byproducts, and the incineration of various materials contribute to the contamination of landfills and the air with HMs. Agricultural practices, including the use of fertilizers and pesticides containing HMs, along with livestock excreting HMs from tainted feed, introduce these pollutants into the soil. HM-containing engineered nanomaterials enter the soils as a component of biosolids or agrochemical formulations of pesticides and fertilizers, either as the active ingredient or as a preservative. Nano-HMs may also be derived from wastewater streams, sewage sludge applications, electroplating, metal finishing, personal care products, fabrics, paints, and the packaging industry [5]. Moreover, atmospheric deposition, resulting from industrial emissions and the combustion of fossil fuels, leads to the settling of HMs on soil and water bodies through precipitation. Urban runoff, transporting pollutants from roads and urban infrastructure, exacerbates the contamination of soil and water. Additionally, discharges of sewage and wastewater, originating from both industrial and urban sources, can introduce HMs into aquatic ecosystems if not appropriately treated. Accidental releases, including spills and leaks during the transportation or handling of HMs, present immediate threats to the environment. The vital recognition and mitigation of these diverse sources are imperative for mitigating the widespread impact of HM pollution on ecosystems and human well-being [6,7].

Remote sensing (RS) has revolutionized environmental monitoring by providing a comprehensive perspective of Earth's landscapes and ecosystems. Through the use of satellites, aircraft, Unmanned Aerial Systems (UASs, drones), and other platforms, RS enables gathering valuable data on the environment. It offers a non-invasive and efficient means to detect and monitor environmental impacts across large spatial scales. So far, various sensor technologies have been utilized to detect contamination in soils and vegetation across large areas. These methods enable the remote monitoring of contaminants either directly, through their association with soil components (such as iron oxides, soil organic matter, and clay minerals), or by observing their effects on vegetation [8]. Although several studies exist, this topic has not been extensively reviewed so far. Here, we focus on the role of remote sensing in monitoring terrestrial HMs in soil and vegetation and aim to demonstrate the success of applying RS in analyzing the impacts of HMs on the environment.

To date, the majority of HM studies and reviews address the HMs' sources and adverse effects on humans, animals, plants and microorganisms, as well as techniques or strategies for the remediation of HM-contaminated environments (e.g., Shawai et al. [9]). In the present review, however, we will focus on the spectral footprints of HMs that can help in their detection by proximal and RS techniques. In particular, we focus on various processes of HMs in the environment that can potentially alter the soil and plant spectral signature.

This review is structured as follows: First, HMs' impacts on and relationships with the environment, with focus on soils and vegetation, are clarified (Section 2). Then, the typical lab analysis of ground-collected samples is described, before indirect approaches via spectral analyses are introduced (Section 3). In Section 4, we review the current literature, focusing on the RS of HM content of soils, whereas Section 5 deals with the remote observation of the HM impacts on plants. In Section 6, the current state is discussed, research gaps are identified, and avenues for future research are presented.

Remote Sens. **2024**, 16, 3221 3 of 30

#### 2. Heavy Metals and Their Role in the Environment

According to the definition in the introduction, 51 elements from the periodic system are counted as HMs or metalloids. The environmental sciences typically focus on a few HMs, for example, copper (Cu), zinc (Zn), nickel (Ni), lead (Pb), cadmium (Cd), cobalt (Co), chromium (Cr), and mercury (Hg). Some metalloids, like arsenic (As), are considered in HM studies as well because of their relatively high toxicity [10]. In addition, concerns over rare earth elements are emerging due to the intensified use of these HMs in high-technology fields [11]. As the definitions are not always integrative, some researchers suggest using the term "potentially toxic elements" instead of HMs [12]. Figure 1 depicts the main effects on soils and vegetation in agricultural-, natural- and forest-ecological systems, discussed in the following.

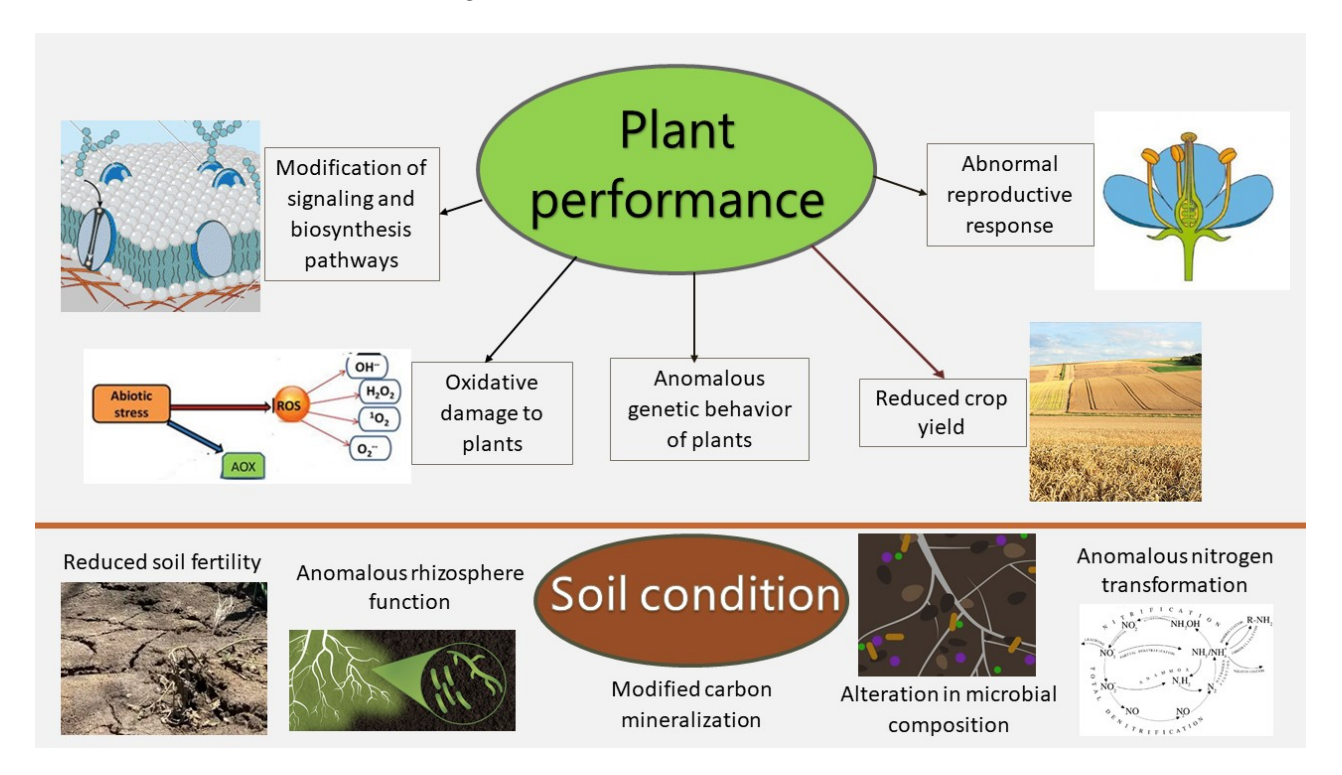


Figure 1. The ecological consequences of HM release in forestry and agriculture. Modified from [13].

Some HMs are essential for nutrition but become toxic when their concentration exceeds the physiological demand of a given organism, e.g., Cu, Zn, and Fe [14]. Multiple consequences arise from high HM concentrations in the environment. Toth et al. [15] report HM soil threshold values of 0.5 (Hg), 1 (Cd), 2 (Sb), 5 (As), 20 (Co), 50 (Ni), 60 (Pb), 100 (Cr, Cu, V), and 200 mg kg $^{-1}$  (Zn). However, such values might still be too high, leading to risk for global food safety. Therefore, regulatory bodies in some countries, like in the European Union, are aiming through various measures within the circular economy to bring down statutory levels for one or more HMs (e.g., Cd and Pb) [16].

The presence of HMs in the environment refers to the concentration, content, and speciation. The HM concentration describes the amount of an HM element in a unit of a substance containing that HM, which is usually used to describe the level of the HM in the substance and thus can be used to compare HM levels among different substances. For instance, the Pb concentration in a soil can be described as mg Pb per kg soil, allowing us to compare Pb levels among different soil orders/soil horizons/regions of soils, and so on. The HM content, on the other hand, describes the total amount of the HM in a given substance with a defined mass or volume. For example, the Pb content can be written in mg or kg in the topsoil (e.g., 30 cm depth) of an agricultural land with an area of, for example, one hectare, giving us an idea of how much Pb is present in the given soil body. The use of the concentration and content can be combined to describe a substance. For instance,

Remote Sens. 2024, 16, 3221 4 of 30

the concentration of an HM in different plant organs/organoids allows us to identify, for example, which organ/organoid can tolerate a high amount of the HM, while the HM content in different organs/organoids shows us the translocation of the HM and which organ/organoid contains/stores the highest amount of the HM. The HMs speciation indicates the chemical form of the HM and thus usually its toxicity in a substance. For example, it is well known that Cr metal and Cr(III) ions are considered non-toxic, while chromate and other Cr(VI) species are highly toxic and carcinogenic [17].

# 2.1. Heavy Metals Impact on Soils

The weathering of rocks and minerals naturally releases HMs into the environment. The crystal structures of the rock-forming primary minerals are made up of oxygen (O), silicon (Si), aluminum (Al), and iron (Fe). HMs can be incorporated into those crystal structures by the substitution of those major constituent ions during rock formation. The degree to which HMs replace the primary constituent ions differs among rocks and minerals. The concentrations and types of HMs in rocks and minerals are thus varied, too. Therefore, the mineralogy or the lithogenic source of soil is the predominant controlling factor for the spatial distribution and the concentrations of HMs worldwide [18]. For example, soils developed on sedimentary phosphate rocks contain thirty-fold U and fifty-fold Cd of soils on black shales [19]. However, HMs in the soil can also originate from volcanic activity or human activities such as mining, gas emissions, energy and fuel production, the use of fertilizers and pesticides, and the generation of municipal waste, among other sources [20]. Compared with the weathering release, the rates of volcanic and anthropogenic inputs of HMs are usually higher and abrupt.

In general, HMs can be flushed into surface or groundwater, absorbed by plants, released into the atmosphere as gases, or semi-permanently bound by soil constituents such as clay or organic material [20]. The soil condition controls the fate of the different HM species, i.e., the state of the soil, including its physical, chemical, and biological characteristics and the processes and interactions that connect them. Here, three main variables, including pH (solubility), ionic strength (activity and charge shielding), and dissolved organic carbon (complex formation), are important. While the toxicokinetics of HMs (the rate at which plants take up and transport HMs) in the rhizosphere is controlled by chemical speciation, the toxicity outcome appears to be determined by toxicodynamics (the dynamic interactions between a biological target, e.g., the plant, and the toxicant, e.g., the absorbed HM species) [5]. The chemical speciation of HMs—the variation in concentration of each HM species as a function of pH [21]—is one of the most important processes controlling the fate of HMs in soil. The effects of HMs on the soil microbial community and the plant uptake, accumulation, and toxicity are mainly controlled by the speciation of HMs [5]. Soils contain a large number of metal-coordinating organic ligands from natural and anthropogenic sources [5]. For example, aliphatic (e.g., oxalic, citric, and saccharic acids) and aromatic (e.g., catechin and hydroquinone allelochemicals) (phyto)siderophores are released by plant roots and microorganisms [22,23]. In addition to those three above-mentioned main variables, there are also several other soil factors, such as available P, oxides, effective cation exchange capacity, moisture content, oxidative-reductive states, and the sorption capacity of HMs, that influence the fate and availability of HMs in soil [20], including their spatial variability [24].

A specific feature of soil pollution by anthropogenic activity arises from the very low rate of soil self-cleaning in concert with human-made emission pathways that are predominantly formed by atmospheric deposition and waste disposal. Due to the various interactions of HMs with organic and inorganic soil constituents, their relatively high charge density, and affinity to soil organic matter, anthropogenic HM inputs typically lead to an enrichment of HMs in topsoil horizons. This enrichment in topsoils forms the basis for pollution detection using direct RS approaches targeting element-specific spectral characteristics [25]. Moreover, topsoils form the most active portion of soil concerning the activity of organisms, above all, the microbes and plants that are physiologically

Remote Sens. 2024, 16, 3221 5 of 30

influenced by the presence of HMs. HM-polluted soils represent very hostile habitats for soil organisms, especially when high HM concentrations are accompanied by low nutrient concentrations [26]. Depending on the element, HMs can exert a strong selective force on microbial communities [27]. There is evidence that HMs negatively impact soil enzyme activity, including urease, catalase, and lipolytic activity, which in turn alters mineralization processes. Zhang and Wang [7] and Enya et al. [28] demonstrated that HMs can slow down the mineralization rate of soil organic carbon, which increases the amounts of soil organic matter in topsoil. Given that soil organic matter plays a fundamental role in soil development and soil physicochemical properties, including soil texture, water holding capacity, and water infiltration, HMs not only impact the elemental composition of a given soil but dramatically alter ecosystem functions that can be monitored by RS. Notably, humus dynamics are governed by litter inputs and annual litter decomposition rates. Consequently, soil humus dynamics often appear to be closely coupled to the composition and density of vegetation [29]. Given that HMs may negatively affect plant growth and vegetation composition, the impact of HM pollution on terrestrial ecosystems is highly scale dependent, offering numerous approaches for RS exploration techniques, targeting direct changes in element contents or indirect anomalies in soil physicochemical properties and vegetation.

# 2.2. Heavy Metals Impact on Vegetation

Elevated levels of HMs in soils can inhibit plant growth and development by disrupting essential physiological processes. The main impacts include the alteration of uptake mechanisms, intracellular processes, signaling pathways, and gene regulation. Those effects are not only visible at the cellular level but also at the whole plant and community level; see Figure 2.

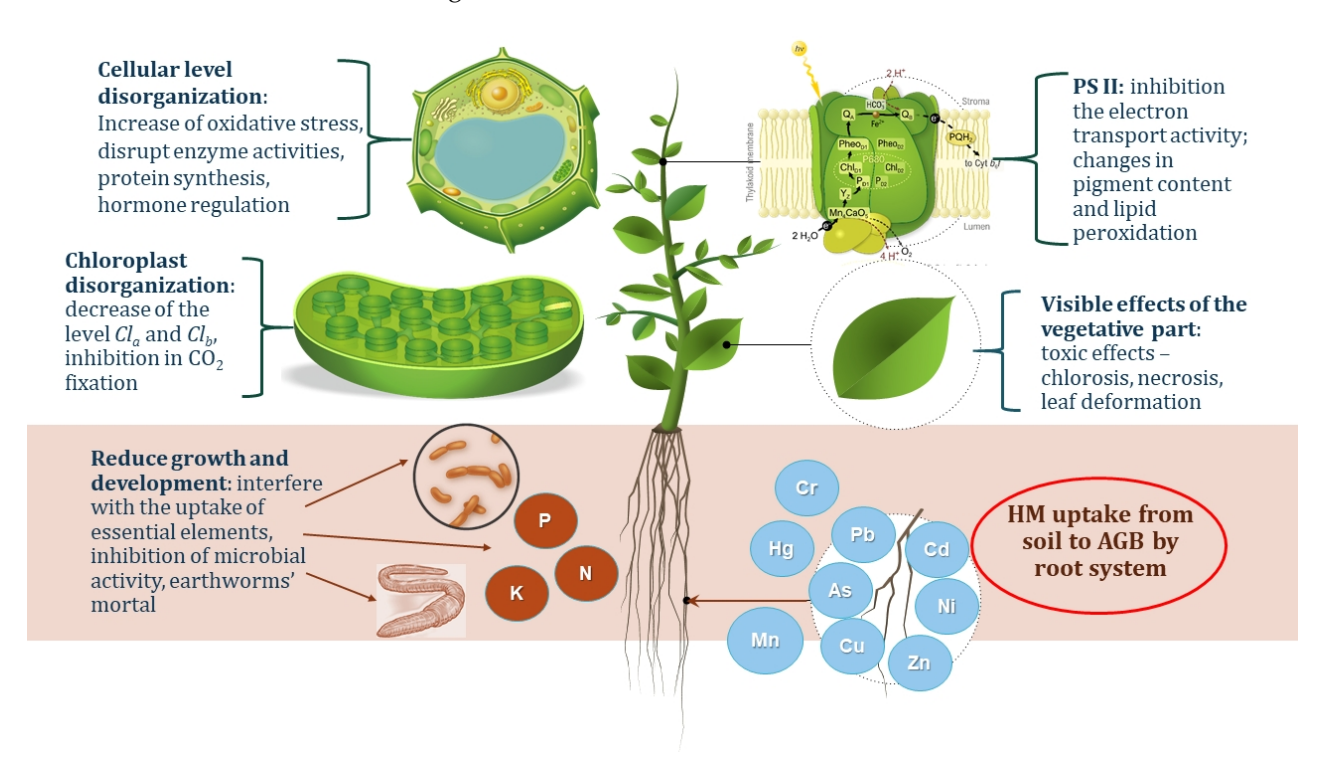


Figure 2. Heavy metals' impact on plants.

HMs are absorbed by plants primarily through various transporters embedded in the root plasma membrane, facilitating their entry into root cells. Metal ion transporters play a crucial role in the uptake kinetics and selectivity of HMs, influencing their accumulation in different plant tissues and organs. The roots are particularly susceptible to reduced elongation, which directly impacts nutrient and water acquisition. For instance, Remote Sens. 2024, 16, 3221 6 of 30

the presence of Cd inhibits root length due to Cd-induced damage to protein structures [30]. Similarly, elevated levels of Mo have been shown to decrease root and hypocotyl (part of the embryonic plant) lengths in plant seedlings and may affect the size of cotyledons (seed leaves) [31].

After entering the plant cell, HMs initiate disruptive intracellular effects, perturbing cellular homeostasis by binding to biomolecules and impeding their functions. These HMs have the tendency to substitute essential ions in enzymatic cofactors, peaking in enzyme inhibition and metabolic derangement. Moreover, HMs cause the production of reactive oxygen species through reactions similar to the Fenton reaction, which leads to oxidative stress and damages important parts of cells like proteins, fats, and DNA. In the root tip and cortical cells, perturbations such as disorganization and denaturation of the nuclear membrane have been observed upon HM exposure [32]. Additionally, Cd exposure has been linked to nitrogen fixation disorders in nodulating plants [33]. These cellular alterations, including the diminution of the main photosynthetic pigments (Cla and Clb), electron transport inhibition, reduced CO<sub>2</sub> fixation, chloroplast disorganization, and photooxidative damage, represent the initial processes subsequent to HM uptake, ultimately resulting in damage to aboveground plant organs [34] (Figure 2).

HM stress triggers a cascade of signaling events in plants involving various signaling molecules and pathways. Phytohormones mediate adaptive responses to HM toxicity, regulating processes such as stomatal closure, root growth inhibition, and antioxidant defense. Moreover, mitogen-activated protein kinase (MAPK) cascades and calcium-dependent signaling pathways modulate gene expression in response to HM stress.

HM exposure also triggers alterations in gene expression profiles, initiating the upregulation or downregulation of specific genes associated with HM detoxification, stress response, and tolerance mechanisms in plants. Those transcription factors play important roles in orchestrating the transcriptional reprogramming necessary for plant adaptation to HM stress. Additionally, epigenetic modifications like DNA methylation, histone acetylation, and microRNA regulation contribute to the dynamic control of gene expression under HM stress conditions. The perturbation of various metabolic processes in plants by HMs, including enzyme activities, protein synthesis, and hormone regulation, can profoundly impact plant growth, reproduction, and responses to environmental stresses [3]. The presence of HMs such as Cu, Pb, and Ni exacerbates oxidative stress through reactive oxygen species formation and heightened DNA damage in plants [34–36]. Moreover, excessive concentrations of HM ions like Cd and Cu in soil can impede polyhydroxybutyrate biodegradation [37]. Additionally, an abundance of Zn in soil exerts cytotoxic effects that disrupt plant metabolic functions, resulting in delays in maturation and growth.

HM contamination can reduce reproductive success in plants by affecting flower development, pollen viability, and seed formation [38,39]. Some studies have shown that HMs (in ascending order: Hg > Cd > Pb > Cu) inhibit the activity of some important enzymes like amylase, lipase, protease, catalase and ribonuclease, consequently reducing seed germination [40]. While low concentrations of Co and Cr accelerate the process of seed germination in some plants, the opposite effect is observed at high doses of these HMs [41,42].

The interaction with soil minerals is one of the crucial factors in the influence of HMs on plant metabolism [43–45]. For HMs that are present as cations in the soil solution, the electrochemical potential gradient at the root cell plasma membranes provides a strong driving force for uptake, and their movement through plants is often mediated by non-selective cation transporters. In particular, Cd and Pb interfere with the uptake, transport, and use of such elements as Ca, Mg, P, and K, as well as water by plants. The inhibition of root Fe(III) reductase induced by Cd can lead to Fe(II) deficiency, which seriously affects photosynthesis and the inhibition of nitrate reductase activity [46]. Excessive Zn in soil can induce Fe deficiency, potentially contributing to the degradation of photosynthetic tissue in plants, as hydrated Zn<sup>2+</sup> and Fe<sup>2+</sup> ions exhibit similar radii [47]. An excess of Zn can cause a deficit of Mn and Cu in plant shoots, which is explained by the difficulty

Remote Sens. 2024, 16, 3221 7 of 30

of transferring these elements from root to shoot. A typical effect of Zn toxicity is the appearance of a purple-red leaf color, which is associated with P deficiency [48,49]. In this way, HMs hamper the uptake and utilization of essential nutrient elements and water and prevent them from participating in physiological processes, eventually leading to chlorosis (yellowing of leaves), necrosis (death of plant tissue), or leaf deformation [50]. These can be considered non-specific stress markers [51], as these effects may be related also to other stress types such as droughts.

However, some plant species have the ability to tolerate HMs and have evolved physiological coping mechanisms to adapt to environments with high element availability in the soil. Generally, these strategies include accumulators and excluders [52–55]. Of the accumulators, specialized (hyper-)accumulators that have evolved in metalliferous environments, of which *Thalaspi cearulenscens* and *Alyssum murale* are the most profoundly studied, accumulate more than 1000 mg kg<sup>-1</sup> of Cd, Ni, and Zn in their shoot dry matter [56,57] without showing significant toxicity symptoms. The ability to accumulate HMs occurs due to the activation of various transporters to relocate the HMs in, for example, vacuoles and through detoxification mechanisms such as binding with histidine [58–60]. In contrast, excluders avoid element toxicity by restricting the entering of HMs at the sites of uptake through extracellular complexation with organic ligands, e.g., sequestration at the cell walls. As a result, HM contamination can also alter the composition and diversity of plant communities by favoring HM-resistant species and genotypes and suppressing sensitive ones.

Generally, the evaluation of individual responses of plant communities to HM pollution must consider individual processes at different time scales, ranging from short-term stress responses in single plant species to long-term adaptation at a community level. Alterations in the ecosystem structure, function, and species composition impact the overall biodiversity and ecosystem services, and anomalies in spectral features may reflect this. Therefore, it seems reasonable to use remote sensing techniques to monitor not only the HM impacts in mesocosm trials but also the vegetation dynamics at a landscape level.

# 3. Ground Sampling and Proximal Sensing in Soils and Vegetation

# 3.1. Soil and Vegetation Sampling

Conventionally, monitoring HMs in large areas requires a well-designed sampling strategy to ensure that the samples are representative of the entire area [61]. Sample handling in the lab includes sample pretreatment such as drying, sieving and homogenizing, purpose-oriented chemical extractions by different reagents, and analysis on various instruments such as atomic absorption spectroscopy, inductively coupled plasma optical emission spectroscopy (ICP-OES), or inductively coupled plasma mass spectrometry (ICP-MS). Some analytical methods, like X-ray fluorescence analysis (XRF), do not require wet chemical pretreatment. These analytical methods determine element-specific spectra of either optical or mass(-to-charge) characteristics, providing information on concentrations of single or multiple elements (for ICP-MS also isotopes). For vegetation samples, special care should be given to avoid contamination by soil particles or other sources and loss of mobile elements during sampling and storage [61]. In addition, the detection limit of an analytical method is a critical factor that determines whether or not and how well HMs can be precisely analyzed. For instance, ICP-MS is capable of analyzing HMs at trace levels with concentrations of ppb (parts per billion) to ppt (parts per trillion) or even below, which is a plausible tool to detect even slightly elevated HMs levels in samples. In general, the conventional methods are relatively time- and effort-consuming. By contrast, RS methods from space and air space allow the rapid tracking of the terrain of large areas without on-site measurement [62]. Nevertheless, a preliminary study of representative field samples of soil and vegetation with respect to their HMs concentrations and basic properties is plausible to validate and elucidate the RS data. Alternatively, proximal sensing offers non-destructive and on-site measurement. It can be carried out alone or in combination

Remote Sens. 2024, 16, 3221 8 of 30

with other RS methods to allow the rapid and precise acquisition of useful information on the investigated areas.

#### 3.2. Proximal Sensing

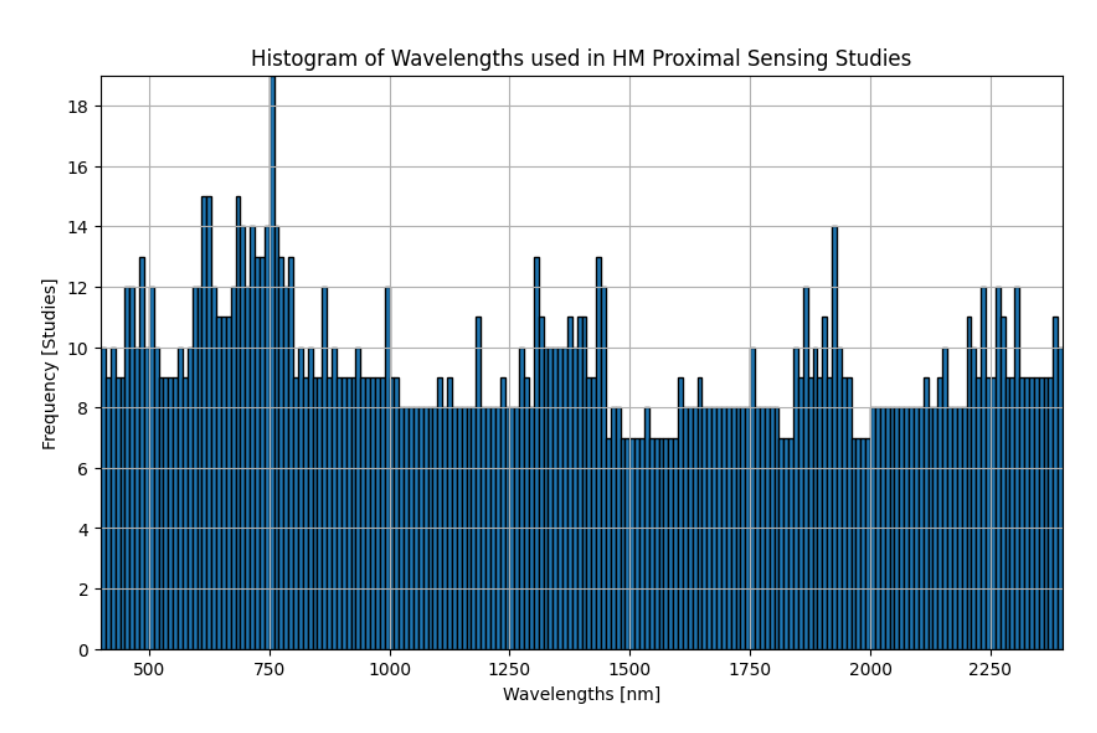
Proximal sensing refers to the collection of data and information about an object or an environment from a short distance, typically within a few meters or centimeters. It utilizes a mobile spectroscopy device moving over a field, recording reflected spectra from the soil or the vegetation, which are then translated into HM concentrations including further important factors such as soil moisture or bulk density. According to Choe et al. [63] and Ning et al. [64], HMs are spectrally featureless in the visible and near-infrared regions of the electromagnetic spectrum. However, the spectral signatures of minerals that bind HMs can be utilized for their indirect detection and mapping using spectral data. This approach offers a valid alternative for estimating HM concentrations over large areas and extended periods [65]. Ultraviolet (UV), visible (Vis), near-infrared reflectance (NIR), and shortwave infrared (SWIR) spectroscopy provides a promising method for the fast estimation of HM concentrations [65–67]. For this purpose, a series of commercial field-portable passive UV/Vis/NIR/SWIR spectroradiometers is used to predict HM contents [68–71]. Devices such as the FieldSpec of Analytical Spectral Devices (ASD) or the PSR-3500 of Spectral Evolution have been successfully utilized to identify HM loads (Table A1). In Figure 3, an example device is depicted. However, adequate devices are quite expensive and require well-trained personnel and stable illumination conditions [72].



Figure 3. Example device: ASD FieldSpec 4 Standard-Res portable spectroradiometer.

Establishing the most effective spectral range is still a controversial issue, as it depends primarily on the HM of focus [73]. Most studies used the 750 nm wavelength and the red and red edge region; see Figure 4. Other studies employed the spectral ranges of 560–620, 860–1100 and 2100–2300 nm to detect HMs [63,74]. However, the spectral ranges for individual HMs may vary in different settings. For example, the spectral characteristics of Cu were found at 480, 500, 610, 750, 860, 1300, 1430, 1920, 2150, and 2260 nm by Song et al. [75], while Omran [76] found that the significant peaks for Cu were at 538, 1259, 1500, and 2184 nm. For the detection of Pb, the wavelengths of either 700–1400 nm [25] or 838, 1930 and 2148 nm [77] are the most sensitive. Yet, other wavelengths have been identified too as shown in Table A1. Typically, the entire visible near-infrared (VNIR) spectral region is used indiscriminately to predict HM concentrations [78–80].

Remote Sens. 2024, 16, 3221 9 of 30



**Figure 4.** Histogram of wavelengths used in proximal sensing studies discussed here (33 studies in total, bins of 10 nm).

The spectral characteristics of soils are influenced by many factors, including soil order, organic matter content, soil moisture, salinity, and bicarbonation. These differences limit the development and application of hyperspectral models. For instance, some researchers have shown that methods using UV/Vis/NIR/SWIR measurements can be used to indirectly assess HMs through the spectral responses of Fe and OM [81,82]. Thus, combining proximal sensing and soil auxiliary attributes could improve HM detection as shown by the estimation of Cr concentrations in the soil [83]. As HM concentrations increase, the soil's spectral reflectance intensity decreases across the entire wavelength range [84]. According to Fu et al. [71], the process of selecting the optimal combination of spectral parameters and models varies for different soil HMs. In a preprocessing approach, Chen et al. [78] excluded spectral bands from the spectrometer intervals of 350–400 nm and 2400–2500 nm to reduce noise and computational cost. Also, Savitzky–Golay smoothing, a widely used spectral processing method, effectively reduces spectral noise during preprocessing. However, there has been limited research on strategies to minimize redundancy in characteristic bands and to extract the unique spectral responses of each HM element [71].

In a similar way, proximal sensing is useful in the assessment of HM concentrations in vegetation under controlled laboratory conditions and in field-scale trials [85–87]. The Red Edge (680–780) range of the electromagnetic spectrum provides key information on the vegetation state. These wavebands showed a significant correlation with HM concentrations in leaves [88]. In a study by Li et al. [87], the spectral characteristics of corn grown in heavy metal-spiked soil were analyzed to develop a new vegetation index for detecting Cu and Pb concentrations in corn leaves. The index that combines the first difference reflectance at 497, 632, and 677 nm wavelengths is the best potential indicator of Cu stress, while the index at 456, 668, and 686 nm wavelengths most strongly indicates Pb stress. Liu et al. [86] presented a method for estimating HM concentrations in crops. It was to determine the levels of Cd and Cu in Oryza sativa L. by upscaling a field-scale HM assessment (FHMA) model from field to regional scale. The FHMA model is based on the link mechanism of soil HM contamination, HM accumulation in crops and HM-induced spectral response. In this study, the HM concentration data in rice are collected and spectral measurements are made by using an ASD FieldSpec Pro spectrometer. The R<sup>2</sup> values for the Cd and Cu were 0.77 and 0.84, respectively. The leaf reflectance of Tilia tomentosa trees was measured using an Remote Sens. 2024, 16, 3221 10 of 30

ASD FieldSpec 3 spectroradiometer (ASD Inc., Longmont, CO, USA) connected to a Plant Probe and Leaf Clip Assembly (ASD Inc., Longmont, CO, USA) [85]. This setup allows for reflectance measurements across a spectral range of 350–2500 nm with a bandwidth of 1 nm. Elevated soil Cd concentrations resulted in significant variations in leaf reflectance, particularly at the 500, 680, and 720 nm bands, while elevated Pb concentrations caused large variations at the 550 and 700 nm bands. In the red-edge region, Cd significantly affected reflectance at the red-edge center ( $\sim$ 720 nm), whereas Pb had a pronounced effect on reflectance from the red absorption to the beginning of the red-edge bands (680 $\sim$ 700 nm). These elevated HM concentrations induced contrasting spectral changes in the red-edge region, likely linked to proportional changes in leaf pigments. Additionally, HM-induced decreases in leaf NIR reflectance are probably associated with alterations in leaf internal structural properties, which reduce internal light scattering and increase leaf transmittance.

Many of the above-mentioned studies focus on the VNIR and, to a lesser extent, the mid- and far-infrared spectroscopy. Maliki et al. [89] and Horta et al. [90] highlighted the potential of VNIR for a near-real-time assessment of various soil components simultaneously and accurately, compared with traditional methods. The performance of VNIR on HM determination seems to rely on the association of HMs and soil organic matter (SOM) and/or Fe as shown in the study of Cheng et al. [66], where the determination of Cd, Cr and As outstripped that of Pb, Cu, and Zn due to the former HMs having a stronger correlation with SOM and Fe, respectively. In addition, VNIR can be combined with mid-infrared spectroscopy (MIR) data, for instance, to detect the concentration of Al, Fe, K, and Ni in soil [91]. It is worth noting that pretreatments of the specimen, such as oven-drying, sieving, grounding, and loss of ignition treatment, can affect the detection results as shown by Kästner et al. [67].

Proximal sensing provides a unique opportunity to combine field and lab measurements with the subsequent development of models for estimating HMs' concentrations in field by spectral analysis. To date there are two main model types to describe the relationship between spectra or spectral features and HM concentrations, namely, statistical descriptions with regressions and machine learning approaches. A number of authors have measured HM concentrations using field spectrometers with the subsequent generation of a partial regression model using the least squares method (PLSR, Partial Least Squares Regression) [69] (Table A1). Other statistical approaches are PCR (Principle Component Regression), OBCA (Optimal Band Combination Algorithm), KS (Kolmogorov–Smirnov Rank), OLS (Ordinary Least Squares estimation method), LRM (Linear Regression Method), or LARS (Least Angle Regression). The advent of machine learning has contributed to enhanced detection accuracy, thereby enabling optical imaging spectroscopy to rival conventional chemical analysis methods in certain scenarios [92]. The careful selection of appropriate input descriptors (features) is crucial for enhancing the accuracy of machine learning prediction models and identifying the key features that impact adsorbent capacity and selectivity. Important methods for interpreting data on HM content include RFR (Random Forest Regression), BPNN (Back Propagation Neural Network), ANN (Artificial Neural Network), SVR (Support Vector Regression), and GA (Genetic Algorithm). Also, combined statistical-AI methods have been implemented, such as the GBRT (Gradient Boosting Regression Tree) coupled to a CARS (Competitive Adaptive Reweighted Sampling) approach [8,93–95].

As a synthesis of the studies reviewed above, there are clear measurement standards to obtain high-accuracy spectra from soil and vegetation, but there is no common standard to identify HM concentrations from these spectra. As the background spectra of different samples are already changing by external and internal factors, for soils, for example, by moisture, organic matter content, texture, etc., the effects of HMs changing these spectra is still not yet clarified. Moreover, absorption features related to specific HMs and their impact cannot be identified; see Table A1.

Remote Sens. 2024, 16, 3221 11 of 30

# 4. Remote Sensing of Soil Heavy Metal Content

Mapping the spatial distributions of various HMs in soils holds significance owing to their diverse bioavailabilities and toxicities [96]. Given the limitation of conventional soil HM mapping based on field sampling and subsequent lab analysis, as well as proximal sensing, RS can provide cost-effective, repeatable, non-invasive, spatially extensive and contiguous observations. The data obtained by RS can complement field monitoring studies of soil and vegetation characteristics and can reduce the effort required for conventional field surveys to monitor and quantify HM content over a wide range of spatio-temporal scales. Instead of direct measurements of the HM concentrations of a specimen, RS uses spectral signatures associated with HMs in soil and vegetation at a scale from field plots to regional areas, using platforms including satellites, aircrafts, and UASs. Accordingly, RS can be used to preliminarily assess land characteristics or HM presence over a large area before employing more accurate, yet expensive, conventional monitoring methods. To date, spaceborne multispectral and hyperspectral RS data, with spatial resolutions of at best 10 and 30 m, have been employed to facilitate the HM monitoring in soils (see Table A2). Multispectral RS data, such as images from Landsat 7 [97,98], Landsat 8 [94,99–106], Sentinel-2 [107,108], ASTER [109], and SPOT 5 [99], or a combination of some of them [110], have been used to identify various HMs in soil, including As, Cd, Co, Cr, Cu, Fe, Hg, Mn, Ni, Pb, Sb, V, and Zn. Hyperspectral RS data such as those from HyMAP [63,95,111], HySpex [112], Hyperion [112,113], Gaofen-5 [113,114], Ziyuan-1 [95], and UASs [115,116] have been used to detect HMs such as As, Cd, Cu, Pb, Ni, and Zn, in soils. Generally, hyperspectral data have a superior ability to recognize chemical characteristics compared to multispectral data [117,118], due to their spectral resolution, discrimination capability, and information density. Nevertheless, multispectral imaging is more commonly used for HM detection in soils primarily due to its cost-effectiveness, lower data volume and processing, established technics and tools, operational efficiency, and sufficiency for HM detection despite the superior spectral resolution of hyperspectral imaging.

These studies have been conducted across various locations, including agriculture soils [107,108,119], roadside [100] and urban areas [115], floodplains [111], as well as mining sites [63,100,120,121], showing the capability of RS in monitoring a wide range of soil and environmental conditions.

Several studies exploit the relationship between soil HM content and spectra of the growing vegetation, e.g., in cropped soils [63,73]. Lassalle et al. [112] processed hyperspectral images obtained by the airborne HySpex VNIR-1600 sensor to map the content of Cr, Cu, Ni, and Zn in soil by correlating vegetation reflectance with HM content in leaves. Guan et al. [105] proposed leveraging the Normalized Difference Vegetation Index (NDVI) calculated from Landsat-8 data as a tool to construct regression models for forecasting the presence and dispersion of HMs in soils.

Specific spectral metrics such as the ratio of specific wavelengths, absorption areas, and asymmetry of absorption features obtained from RS data, are identified as indicative of HMs' (i.e., Pb, Zn, As, and Cu) presence. Accordingly, various statistical and machine learning algorithms, such as Partial Least Squares Regression (PLSR) [95,98,102,105,108,113], Multiple Linear Regression (MLR) [63,107,112], Random Forest Regression (RFR) [98,99,104,106,108], Genetic Algorithm (GA) optimization [95,100,101], Gradient Boosting Regression Tree, Artificial Neural Network (ANN) [102], Reference Vector Regression (RVR) [102], Back Propagation Neural Network (BPNN) [103,108], and geostatistical interpolation techniques [103] are employed to establish relationships between hyperspectral signatures and HM concentrations. Each of these models may differ in performance for specific HM concentrations in soil. To analyze the bioaccumulation characteristics of Cr, Cu, Ni, and Zn in soil-rice systems, Xie et al. [122] used MLR, Support Vector Regressions (SVR), RFR, and Cubist. Their research demonstrated the feasibility and benefits of using machine learning techniques, particularly RFR, to estimate HM accumulation in soil-rice systems, showing superiority over traditional statistical methods like MLR. Tan et al. [119] showed that CARS-Stacking method has a better performance in retrieving As, Cr, Pb, and Zn concentration based on their hyperspecral features, compared to other conventional methods such as RFR, BPNN, SVR, k-Nearest Neighbor (k-NN), Remote Sens. 2024, 16, 3221 12 of 30

and Extreme Learning Machine (ELM). In the study conducted by [106], multiple sources of geographical data were utilized to establish three temporal indices that characterize the temporal enrichment process of soil HMs. Additionally, temporal-spatial-spectral (TSS) covariate combinations were constructed. The researchers employed the random forest algorithm to map soil HMs at a regional scale. Notably, these mapping results for Pb obtained in their study outperformed other mapping methods, including ordinary kriging, ANN, and multivariate linear regression methods.

In spatial mapping of Zn in urban soil using Landsat data, Shi et al. [99] showed that RFR may give more robust results compared to the geographically weighted regression (GWR) method. Shi et al. [104] proposed a hybrid artificial intelligence model, termed LASSO-GA-BPNN, integrating LASSO, genetic algorithm, and BPNN for estimating soil HM content in Huanghua, China, using RS data. LASSO (Least Absolute Shrinkage and Selection Operator) is a statistical method whose main purpose is the feature selection and regularization of data models. This approach significantly enhanced the accuracy and generalization of Ni, Pb, Cr, Hg, Cd, As, Cu, and Zn content estimation and outperformed SVR, RFR, and spatial interpolation methods. Even transfer learning was applied by Yang et al. [101] to use training features of one year to link with target features of another year by similarity analysis.

Moreover, researchers have shown that integrating RS data with ancillary data such as soil properties, geology [99], land use/land cover [103], topography [123], vegetation indices [99], and Geographic Information System (GIS) data can play a key role to enhance the accuracy of HM detection models. RS not only can be used for direct HM detection in soils by analyzing spectral signatures of HMs but also indirectly by identifying associated geological alteration zones and structural features. Beygi et al. [109] demonstrated the use of ASTER satellite imagery and various image processing techniques to identify the high to moderate fracture density zones associated with the identified alteration zones in Argillic, Phyllic, and Propylitic rocks indicating the distribution high potential zones for copper mineralization. Moradpour et al. [124] utilized Landsat-7 and ASTER images to map propylitic alteration zones and geological structures, identifying high-potential zones for iron skarn mineralization in the Galali region, Iran. As HM contamination spreads via fluvial phase and accumulates with natural sediments, topography can also be an important predictor for spatial HM patterns [123].

Despite advancements in the application of remote sensing data for HM detection, significant challenges remain. In quantitative uses of hyperspectral RS data, the influence of hyperspectral bands varies, and incorrect classification of bare soil images leading to abnormal prediction values is a significant issue. Although fusion can be seen as a technique for combining images to achieve higher spatial, spectral, and temporal resolution [110,125], differences in spectral and spatial resolution between ground sampling and RS data remains challenging. The need for (atmospheric, radiometric, spatial, etc.) correction methods, and the difficulty in detecting HMs at low concentrations [73], have to be considered. Increasing moisture, for example in floodplains and lowlands, reduces satellite reflectance spectra, complicating detection [98]. Dynamics in land use/land cover and biodiversity can also affect spectral reflectance and the accuracy of RS monitoring, highlighting the necessity for multisource remote sensing data and stereoscopic monitoring methods [121]. Multispectral images used in many studies lack the spectral resolution needed to accurately represent the spatial patterns of soil HMs. Techniques such as spectral unmixing are applied to enhance the spatial resolution of hyperspectral data, improving the accuracy of estimation by isolating purer soil spectra. This is particularly relevant for airand spaceborne hyperspectral data where mixed pixels are common. Besides limited spectral bands, challenges such as cloud cover and soil contaminants hinder the effectiveness of RS methods [126]. The studies consistently validate their models by comparing results with ground measurements, demonstrating the reliability of the remote sensing-based estimations. However, ground referencing is crucial for assessing the accuracy and effectiveness of the developed models. These issues underscore the need for improved spectral

Remote Sens. 2024, 16, 3221 13 of 30

precision, detection methodologies, and inversion models to enhance RS capabilities for HM detection in soil.

# 5. Remote Sensing of Heavy Metal Impact on Vegetation

The exposure of plants to HM pollution induces physiological changes that can alter their spectral properties. As outlined in Section 2.2, HMs can induce stress symptoms such as chlorosis and necrosis, which can significantly impact the absorption and reflection of light by plant leaves [60,127,128]. Not only can these extreme changes in reflectance patterns be detected and quantified using RS techniques but also smaller impacts such as minor changes to the leaf structure and pigment composition may be visible by RS. For instance, hyperspectral measurements are sensitive to subtle differences in the plant response to environmental stressors [129]. Therefore, a plant exposed to HM stress is expected to exhibit differences in its spectral signature compared to a healthy plant [130]. Moreover, analyzing the leaf spectral response allows for the investigation of biochemical and morphological changes induced by HM stress [131]. An in-field spectroscopy was conducted by [130] to assess and estimate concentrations of HMs [namely: Cu, Zn, Pb, Cr, and Cd] in grapevine foliage in Iran. They further compared the effectiveness of SVR and MLR algorithms in modeling the relationships between foliar spectral responses and HM concentrations. They compared the average reflectance spectra of healthy versus HM-stressed grapevine leaves (Figure 5). Based on their observations, in the visible part of the spectrum, there is a notable decrease in the light absorption rate for stressed grapevines. This is attributed to the fact that the spectral characteristics in this region are largely influenced by plant pigments [129], suggesting that HM stress leads to a reduction in pigment content. Moreover, differences in spectral characteristics between healthy and stressed leaves are observed in NIR and SWIR regions (Figure 5), mostly being influenced by the change in leaf structure and water content [129]. According to the findings in [130], healthy grapevine leaves exhibit lower reflectance in the visible, NIR and SWIR regions compared to stressed leaves. Although this study did not investigate other properties of grapevine (e.g., leaf chlorophyll content, LAI, and leaf water content), it can be inferred that HM stress could significantly impact them.

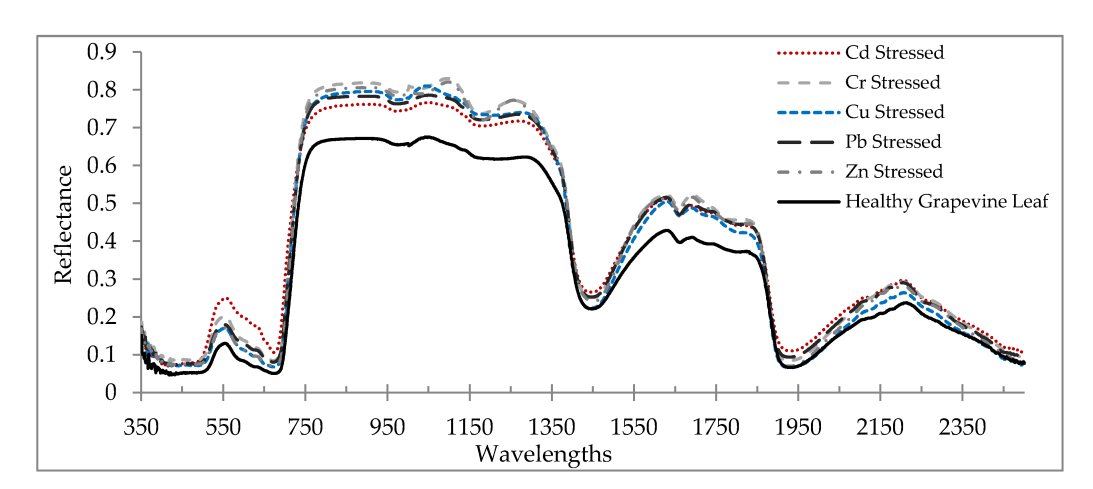


**Figure 5.** Comparison of the average reflectance spectrum between healthy grapevine leaves and those stressed by HMs (reprinted with permission from Mirzaei et al. [130] under the Creative Commons Attribution (CC BY 4.0) license).

Various methods have been employed to study the relationship between HM and RS data. The studies listed in Table A3 can be separated into three general categories, either by using spectral indices, by exploiting a direct relationship between HMs and RS data, or by transferring the knowledge obtained with ground-based measurements to the RS scale. In such three categories, statistical approaches, physical models, and machine learning methods have been employed to link several co-variants to target samples containing HMs (Figure 6).

Remote Sens. 2024, 16, 3221 14 of 30

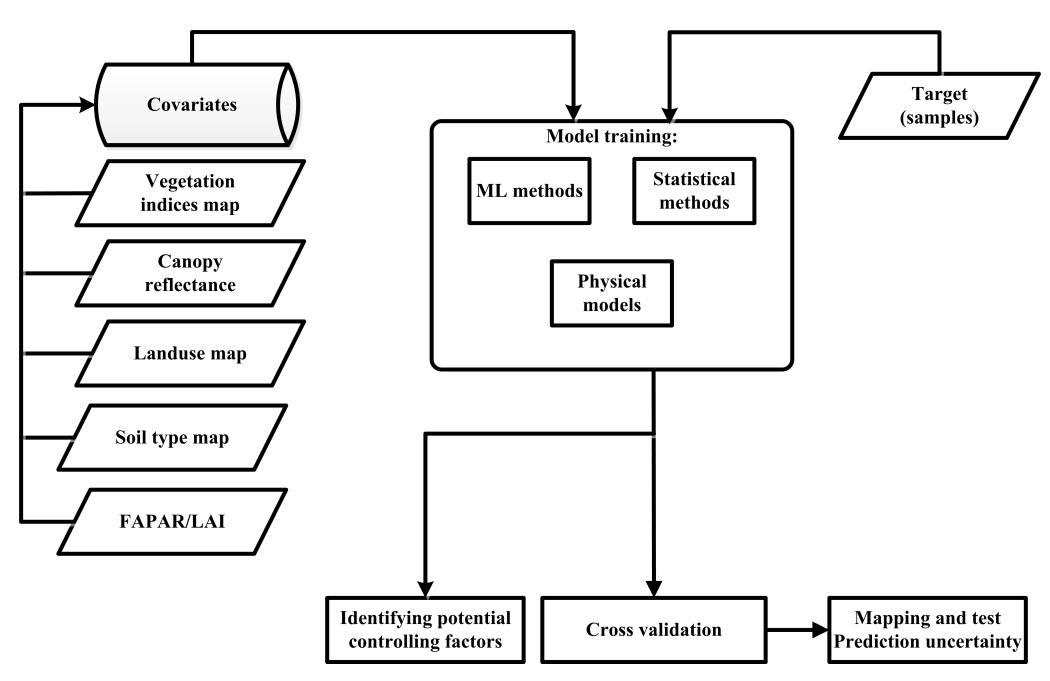


**Figure 6.** Typical implementation of statistical approaches, physical models, or machine learning methods to link different covariates to target soil or vegetation samples containing various levels of HM content.

#### 5.1. Utilizing Spectral Indices

Several studies demonstrated the effectiveness of spectral indices in detecting HM pollution using RS data. Mikkola [132] used time series of NDVI, calculated from Landsat data, to observe changes in vegetation health across different years in Russia to explore the environmental impact of HM emissions from Ni and Cu smelters. They found that the severely damaged areas near the pollution source doubled in ten years. Zhang et al. [133] utilized HyMap and Hyperion images to calculate three indices, with the Vegetation Inferiority Index (VII) identified as a better indicator of vegetation changes due to HM pollutants compared to NDVI. D'Emilio et al. [97] demonstrated the correlations between NDVI values, calculated from Landsat 7 data, and nine measured soil HMs (Cd, Co, Cr, Cu, Fe, Mn, Ni, Pb and Zn), in the vegetated area of Southern Italy. They provided valuable insights for cost-effective monitoring procedures by preliminary screening of potentially contaminated areas based on NDVI. Liu et al. [126] used Enhanced Vegetation Index (EVI) from HJ-1A/B multispectral images to assess Cd, Pb, and As contamination in four rice fields under two mild and severe levels near the Xiangjiang River in China. They found that the rice phenology was affected more in the severe stress class. Zou et al. [134] employed the enhanced spatial and temporal adaptive reflectance fusion model (ESTARFM) to fuse MODIS and Landsat images, and derived NDWI and EVI indices to generate a rice phenological feature space scatter diagram. This diagram provided the rice Growth Rate Fuctuation Index (GRFI). The GRFI increased with the increasing Cd stress level, and therefore, it effectively differentiated the stress levels based on the phenology of the rice growth. The ESTARFM was also used by Zhang et al. [135] to fuse MODIS and Landsat 8 images. They derived time series of NDVI and NDWI to study specific rice phenometrics (e.g., the tillering date, middle heading date, maturity date, growth season length, vegetative phase length, and reproductive phase length) in Zhuzhou City, China. A relative phenophase index (RPI) was introduced to identify rice paddies under HMs (e.g., Cd, Hg, Pb, and As content) stress levels. Zhang et al. [135] proposed a new vegetation index, called the heavy metal stress sensitive index (HMSSI) as a ratio of red-edge chlorophyll index (CIred-edge) and the plant senescence reflectance index (PSRI). These three indices have been derived from Sentinel-2 images during different rice growth stages to detect HMs (Cd, Hg, and Pb) in China. They found that HMSSI outperformed CIrededge and PSRI. Liu et al. [136] investigated the Cd stress on rice in China using integrated

Remote Sens. 2024, 16, 3221 15 of 30

HJ-1A/B, Landsat 7, and Landsat 8 images to generate NDVI time series as a rice phenological indicator. The Dry Weight of Roots (DWRT) was simulated using the World Food Study (WOFOST) model. A feature space was established based on the phenological indicator and DWRT to monitor Cd stress levels with an accuracy of over 95% for distinguishing the severe stress level. Zhang et al. [137] analyzed the Cu Stress Vegetation Index (CSVI) calculated from the Hyperion hyperspectral image and showed the correlation between CSVI and measured leaf Cu concentration. In another study, Liu et al. [138] used a coupled leaf canopy radiative transfer with the WOFOST model to simulate the EVI index in the rice-growing region in China, and in parallel, they derived EVI from fused (using ESTARFM) MODIS and Landsat. Finally, they introduced an Area Wavelet Transform Stress signal (AWTS), based on an EVI, to detect rice under Cd stress and explore its spatio-temporal variation. Tang et al. [139] employed the WOFOST model to simulate the time series of Leaf Area Index (LAI) during the crop growth period in China to investigate HM stress in rice. A new stress index based on spatial and temporal characteristics (SIST) was established to assess HM stress levels at the regional scale, implementing the spatial autocorrelation and temporal dissimilarity of LAI. They reported a strong correlation (82%) between SIST and the measured soil Cd content. Ma et al. [140] used MODIS NDVI and the Sentinel-2-derived MERIS Terrestrial Chlorophyll Index (MTCI) to study the impact of mining activities on the vegetation change in six mining areas in China. They reported significant vegetation degradation and chlorophyll content reduction in some mining areas, attributed to HM pollution. Zhang et al. [141] implemented a gated recurrent unit (GRU) neural network algorithm to study the annual spatial distribution of rice under Cd metal stress in Zhuzhou, China. Eight vegetation indices (REP, CIred-edge, MSR, MCARI, NDVI, RDVI, and NDRE) were derived from Sentinel-2 and utilized in the random forest algorithm. Such indices were added to the GRU model to generate an annual classified map of HM-stressed rice areas with an accuracy of over 80%. Kayet et al. [142] combined nine different vegetation indices to map the vegetation stress index and identified its correlation with the distance from the coalfield in Jharia, India. They obtained these indices from the bands of airborne AVIRIS-NG hyperspectral imagery. The indices were sensitive to different factors and included NDVI (greenness), NSI (nitrogen content), SR (chlorophyll), SWSI (water content/chlorophyll), SRWI (leaf water potential), NWI (canopy water status), CSVI (copper content), HMSSI (cadmium content), and ARI (leaf anthocyanin pigments). The study found a negative correlation between the distance of vegetation from the coalfield and the vegetation stress index.

# 5.2. Exploiting the Relationship between Spectral Characteristics or Indices and HMs

Several studies focused on defining the estimation models between the leaf and soil HM concentrations and RS image spectra to map the spatial distribution of HMs. Qu et al. [143] built an estimation model by employing multiple linear regression between the measured Cu concentrations in leaves and spectral information extracted from the HJ-1 hyperspectral image to imagine the spatial distribution of Cu in vegetation. Liu et al. [138] adopted the Bayesian method integrated with Sentinel-2 images to identify Cd stress in rice crops at a regional scale in China. The unstressed and stressed (including HMs, diseases, nutrients, and pest stress) rice were obtained by applying the Support Vector Regression (SVR) on the multitemporal normalized difference red-edge index (NDRE) calculated from Sentinel-2. The Bayesian method was then used to map the probability of rice being stressed by Cd pollution with an accuracy of 81.57%. Yang et al. [144] used the random forest inversion model using the bands of Headwall and Hyspex (airborne hyperspectral images) and measured soil HMs (Cu, Zn, As, Sn, Cr, and Cd) to obtain their spatial patterns. The NDVI, which was calculated from the image, was used to evaluate plant health under different HM concentrations. Li et al. [92] examined Cd stress to plants using a time series of the fraction of absorbed photosynthetically active radiation (FAPAR) retrieved from Sentinel-2 images implementing the radiative transfer model. A stress index (SI) was calculated based on the decomposition of time series of the FAPAR signal (that reflected only HM stress) using the CEEM-DAN (complete ensemble empirical mode decomposition with adaptive noise) method and local spatio-temporal Moran index

Remote Sens. 2024, 16, 3221 16 of 30

reflecting autocorrelation. A positive correlation of SI with field-measured Cd concentrations was successfully established. Zhong et al. [145] used Genetic Algorithm optimized Partial Least Squares Regression (GA-PLSR) to establish the estimation models of the measured soil Cd and As concentrations with HJ-1A hyperspectral spectra to identify the areas contaminated with HMs.

# 5.3. Knowledge Transfer from Laboratory/Field Measurements to Remote Sensing Scale

Several studies highlighted the transfer of knowledge from laboratory or field to RS data to map the spatial distribution of HMs. Khalili et al. [146] categorized the signature obtained from a field spectroradiometer for healthy and unhealthy leaves (contaminated by As and Pb) and utilized this knowledge in a spectral angle mapper to classify Hyperion hyperspectral image to obtain the spatial distribution of HMs. Hede et al. [147] developed a new vegetation index called VIGS (Vegetation Index considering Greenness and Shortwave infrared) to detect vegetation anomalies due to soil HMs in areas covered by thick vegetation. The study conducted laboratory experiments to demonstrate the capability of VIGS, which investigated changes in leaf reflectance spectra based on the concentrations of four selected HMs (Cu, Pb, Zn, and Cd) in soils. The VIGS index was calculated for large region in Jambi, central Sumatra, Indonesia, utilizing the bands of Landsat 7. For comparison purposes, the NDVI index was also obtained. The correlation between HM contents, prepared by kriging interpolation of spatially distributed measurements, and indices showed that VIGS was more sensitive to vegetation stress than NDVI. Jin et al. [148] introduced a theoretical model with a triangular plane to assess the relationship between the differences in air temperature (Ta) and canopy temperature (Tc), and LAI as indicators of HM stress in rice crops. They developed a new Normalized Heavy-Metal Stress Index (HMSI) based on the relative positions of Tc-Ta and rice LAI within the triangle plane. The model was validated using Tc-Ta and LAI measurements from various stress levels of HMs (soil Cd, Hg, and Pb content) in rice fields in China, confirming the reliability of HMSI in assessing HM stress levels. Additionally, Landsat 8 bands were utilized to derive Tc-Ta (from thermal bands) and LAI (from green normalized vegetation index (GNDVI)), and the triangular model and HMSI were applied at a regional scale with promising accuracy in assessing HM stress levels across the region. Wu et al. [149] made use of the PROSAIL model through a global sensitivity analysis in rice fields in China to understand the most sensitive vegetation parameter to Cd stress levels. They found that the chlorophyll content is the most sensitive one for detecting rice canopy Cd stress. According to this, they suggested a new vegetation index, named Heavy Metal Cd Stress-sensitive Spectral Index (HCSI), to detect Cd stress in rice at a regional scale using Sentinel-2 images. Li et al. [150] optimized the chlorophyll (vegetation) index (NVI) based on the measured leaf Pb content, chlorophyll content, and field leaf spectra, and further calculated this optimized index from the HJ-1A hyperspectral image to assess the spatial distribution of Pb stress levels. Lassalle et al. [112] optimized NDVI for four measured HMs (Cr, Cu, Ni, and Zn) based on the highest correlation between each measured HM and the red and near-infra-red bands of measured leaf spectra using the field spectroradiometer. This knowledge was transferred to the HySpec image to obtain spatial optimized NDVI, and demonstrated the potential of hyperspectral remote sensing to assess plant metal uptake. Li et al. [151] performed the domain adaptation method to align the distributions (reduction in distance) of the source domain (laboratory spectral data of leaves) with those of the target domain (spectral data of Gaofen 5-02 and Zhuhai-1 OHS-3D hyperspectral images). Three regression methods (Ridge, LASSO, and PLSR) were employed and compared to establish HM (Cu, Zn, Cd, and Pb) prediction models using the domain-adapted source domain. The domain-adapted target domain was then substituted into the prediction models, facilitating the scaling of prediction models from laboratory to satellite images. The study concluded that Ridge and LASSO were more effective compared to PLSR.

Remote Sens. 2024, 16, 3221 17 of 30

#### 6. Current State, Perspective and Way Forward

#### 6.1. Current State

RS has been an indispensable opportunity for environmental HM monitoring, for example, in mining areas [121,152]. It can comprehensively, rapidly, and continuously identify the environmental factors and the monitoring of those ecological changes related to HMs in plants and soils [121]. Multi- and hyperspectral sensors from aircraft and satellites have been employed to link spectral information to HM content or concentrations. It is remarkable that most studies have been conducted for Chinese sites, where several areas with HM pollution exist. The evolution from multispectral to hyperspectral imaging has significantly enhanced the ability to detect specific stress signatures in vegetation induced by HMs. Early methods relied on basic vegetation indices such as NDVI, which provided general indicators of plant health but lacked the specificity to detect HM-induced stress accurately. Advanced relevant indices like the HMSSI and CSVI have been developed to enhance sensitivity to specific HMs [135,137]. Advancements in hyperspectral imaging have allowed for the detection of subtle spectral changes associated with specific HMs, improving both detection rates and accuracy. More recent research (e.g., [138]) emphasizes the integration of machine learning to interpret increasingly complex datasets, reflecting a shift towards more predictive and dynamic environmental monitoring.

In order to determine the amount and distribution of HMs in space, most scientists are increasingly using AI methods, such as RFR or GA, either combined with statistical approaches or applied alone [104]. While substantial progress has been made in detecting HM pollution in vegetation using RS, several challenges still exist as outlined by Li et al. [152]: (1) sensor characteristics, (2) the integrated utilization of multiple RS datasets, (3) uncertainty in the RS of HM proxy variables, (4) scaling effect problems, (5) low degree of automation, (6) the lack of computational power for massive RS data, and (7) weak forecasting and comprehensive analysis.

Examples of these challenges have been identified in the studies reviewed above. Regarding (1), multispectral sensors are able to detect altered vegetation characteristics, e.g., due to reduced chlorophyll content under HM impact, but the predictive skill to provide further information about the concentration or type of HM is limited. For (2), it is well known that data fusion integrates two or more data types with different spectral and spatial features that can improve performance. The new product contains all features of all individual datasets but with more pixels of higher spatial, spectral, and temporal resolutions, hence being more informative. However, finding an appropriate satellite image that has been taken as simultaneously as possible to the sampling campaigns can be challenging [110]. The challenge (3) comes from the fact that not all HMs have their own unique spectral response and that for some HMs, only at sufficiently large concentrations can a subtle disparity be observed in the spectral responses. Hence, their detection relies on their co-variation with the spectrally responsive HMs. The closeness of a correlation dictates the accuracy of a prediction [73]. Without any theoretical grounding, this correlation is thus site specific and not widely applicable. Here also, the preprocessing is essential because in quantitative applications of RS for HM content, the contribution of spectral bands is different. Abnormal prediction values, e.g., resulting from incorrectly identified bare soil conditions, are a major problem [114]. Regarding (4), spaceborne and airborne RS both face their own limitations with respect to either the spatial resolution or area size covered. Spaceborne hyperspectral imaging with fast data acquisition and a low occurrence period enables low-cost monitoring at large scales but with a limitation on resolutions of 10 to 30 m, at best. Airborne hyperspectral data, from sensors equipped on balloons, helicopters, or airplanes, can be a candidate solution to overcome imaging spectral and spatial resolution limitations. However, airborne RS is limited due to its small spatial coverage during the traveling time of the aircraft and to few occasions due to flight costs. The problem of (5) originates from the fact that most research works on the RS of HMs are individual studies with limited spatial extent and transferability to other regions. Therefore, the automation of processes is typically not foreseen and bears further

Remote Sens. 2024, 16, 3221 18 of 30

risks. Point (6) should no longer be a challenge, as computational power is more and more accessible to users, with cloud processing platforms from private (Google [153], AWS, and Microsoft [154]) or public (CODE-DE [155] and DIAS [156]) actors. This is especially true for multispectral RS data, but hyperspectral observations can barely be found in these repositories and need to be uploaded manually. However, this is also currently changing, as Earth Observation Laboratory (EO-LAB) (https://eo-lab.org, accessed on 20 August 2024) as a RS data provider and processing facility will provide EnMAP data soon. Finally (7), according to [152], the RS of the environment has predominantly focused on monitoring rather than adequately predicting environmental trends. There remains a significant gap in the overall comprehensive ability or global framework to analyze environmental quality and status based on RS data.

# 6.2. Perspective and Way Forward

As current relationships between spectral observations and HM concentrations have been described based on statistics or AI, they have not been physically modeled so far. Here, a more thorough understanding of the related processes is needed to bring the relationships to another level of detail. This can be achieved by a physical HM-related model in combination with a radiative transfer model. An example blueprint can be the forward calculation of leaf spectra based on leaf N content, where its inversion uses hyperspectral observations to retrieve the N content; see the work of Dehghan-Shoar et al. [157]. This could also increase the transferability to regions where the regression and AI-based approaches as they are used now may not be suitable. Initial work has been published so far, e.g., the study by Liu et al. [136] utilizing the WOFOST crop growth model. They relied mainly on LAI and optical indices simulations, but WOFOST has the potential to simulate crop photosynthesis, biomass, and water use. Considering these variables could potentially provide additional insights into the HM impacts on vegetation properties, functioning, and yield.

Another aspect is the interaction with other compartments of the environment. For instance, upon soil moisture change, the dissolved HM concentration may vary [158], leading to a different risk posed for vegetation and to leaching into a water body. Soil moisture and electrical conductivity as indirect measures of soil salinity are both well-established observables from remote sensors [159–161]. These could be considered as additional information sources for the determination of HMs from remote sensing.

The development of standardized protocols is another recommendation. By doing so, the fast and accurate forecasting of the level of HMs in the landscape is possible to ensure a functioning ecosystem. At the same time, understanding all processes of the spatial distribution of HMs in the environment from the source through air- and fluvial depositions of HM-contaminated sediments will help identify contaminated regions. It is worth noting that the soil spectral features revealed by RS are not limited to the variation in the mineralogy of the soil but are also applicable to the elevated HMs concentrations of anthropogenic sources. Therefore, other parameters, such as means and velocity of HMs transport, weather and climate conditions, specific features of the HMs source and sink, etc., are to be included in analyzing the RS data. For example, when an HM is transported from an anthropogenic source to a soil at a particular location, the main transport mechanisms are likely to include, but not be limited to, moving air currents and dust deposition, moving water in the form of runoff or flooding, massive movement of soil materials due to gravity, and intentional spreading by tractors, sprayers, manure spreaders, trucks, etc. [18,162]. Therefore, distance from the source of HM-containing materials, wind direction flowing over that source, the presence of water reservoirs, etc., should be used when modeling HM concentrations through RS data. Precipitation in areas with active HM sources within a few kilometers of the source should also be considered as a potential covariate for this type of modeling, as dry and wet depositions of atmospheric HMs are among the most widespread forms of soil contamination, especially for arable land [18]. In addition, features of, for example, livestock manure, sewage sludge, inorganic fertilizers, and agricultural chemicals, Remote Sens. 2024, 16, 3221 19 of 30

as well as industrial contaminants, should be included in estimating HMs using RS data. This general recommendation about investigating in a physical process description related to HM impacts on spectra as well as to its spatial distribution in the environment could lead to initial research on physics-induced or explainable artificial intelligence, as "traditional" AI is already heavily used for this purpose. In general, future work should elaborate toward a paradigm shift in approaching the HM problem away from regression analyses and toward a holistic understanding of processes, which may improve the monitoring and detection of HMs.

Another aspect that future research should target is the discrimination to other vegetation stress types such as droughts, salinity, or nutrient deficiency, or combinations of them. The increasing severity of droughts due to climate change as well as salinity during agricultural practices may show the same alterations in plant physiology in many parts of the world, such as reduced chlorophyll content. Both HM-related and other stress types can have joint impacts, as, for example, the resilience to droughts may be reduced due to HM exposure. Current research mainly focuses on single snapshots in time with single RS observations, but the overall evolution of HM impacts may be better observed by analyzing time series data. Those more longitudinal studies are able to track changes over time, allowing for better understanding the long-term effects of HMs accumulation in vegetated ecosystems. Moreover, we may need to increase the sample size and its heterogeneity, where AI may help in disentangling effects if the data source is large enough. Auxiliary data in addition to HM concentrations are soil texture and moisture, vegetation species, etc., to help disentangle the HM impact from other stressors. Here, an extension to other areas outside China could enrich the diversity of impacts. There is a scarcity of data from other countries, where industrial pollution also poses a significant risk to vegetated ecosystems, to have a fair representation of impacts at the global scale.

Finally, new airborne sensors and satellite missions are in development, improving the detection of HM impacts on soils and vegetation. An important initiative to note is the ESA Copernicus Hyperspectral Imaging Mission for the Environment (CHIME), which will deploy a specialized visible-to-shortwave infrared spectrometer for regular hyperspectral observations. Likewise, NASA's Surface Biology and Geology (SBG) mission aims to assess biological, physical, chemical, and mineralogical characteristics of the earth's surface, with specific capabilities for detecting HMs. Also, private companies are taking the step toward hyperspectral imaging, e.g., Planet with its Tanager constellation (Tanager-1 to be launched by July 2024). Moreover, as HM impacts plant photosynthesis, the resulting solar-induced fluorescence (SIF) may be altered. When photosynthesis occurs, some of the unused energy absorbed from the sun is emitted as heat and also as a glow in the O2-A and O2-B absorption lines at 760.5 nm and 687.5 nm [163]. ESA will launch the dedicated satellite mission FLEX (Fluorescence Explorer) in 2025 [164]. Future continuous spaceborne monitoring will also enable timely interventions and informed decision-making to mitigate the adverse effects of HM pollution. Currently, very few studies employing UAS have been found. As hyperspectral sensors for UAS exist, there is one perspective to perform on-demand hyperspectral surveys or continuous monitoring for HM-contaminated sites. This could reduce the scale mismatch between in situ sampling and remote observations, and enlighten the driving processes in environmental HM impacts. In particular, the implementation of these UAS data in physical simulations from HM impacts on plants and their effects on the reflectance spectra could move the field of research forward.

#### 7. Conclusions

In conclusion, RS offers unprecedented opportunities for the comprehensive assessment of HM impacts on soils and vegetation. Through the integration of various RS platforms, sensor types, and approaches, studies have been able to detect, monitor, and analyze HM contamination with remarkable precision and efficiency. These advancements have significantly contributed to our understanding of the spatial dynamics of HM pollution. However, despite the remarkable progress made in RS applications for HM assessment,

Remote Sens. 2024, 16, 3221 20 of 30

> several challenges remain. For instance, the current research utilizes mainly regression and machine learning methods, without a detailed understanding of the underlying processes that HMs participate in. Several ways forwards have been suggested, with huge benefits expected by more detailed investigations into the causalities and interdependencies of chemical and physical processes with reflectances to be recorded at hyperspectral sensors.

> Although the awareness of HM contamination has risen, related threats to environment and society continue to exist, also because of the high stability of HMs. Addressing the above-mentioned challenges will be critical for advancing the reliability and accuracy of RS-based approaches in monitoring HM impacts on soils and vegetation and to develop effective mitigation strategies.

> Author Contributions: Conceptualization, V.L. and C.M.; methodology, V.L. and C.M.; writing original draft preparation, all authors; writing—review and editing, all authors; visualization, V.L. and B.B.; funding acquisition, V.L. and C.M. All authors have read and agreed to the published version of the manuscript.

> Funding: V.L. and C.M. acknowledge funding by the Initiative and Networking Fund of the German Helmholtz Association (FKZ: GI-038). R.B. acknowledges the Mobility Grant M-0749. C.M. and B.W. received support by the OrganoRice project funded by the German Federal Ministry of Education and Research (BMBF) within the "CLIENT II-International Partnerships for Sustainable Innovations" funding initiative (Grant No. 01LZ1806A).

Conflicts of Interest: The authors declare no conflicts of interest.

Abbreviations					
Acronym	Description				
AI	Artificial Intelligence				
ANN	Artificial Neural Network				
ARI	Anthocyanin Reflectance Index				
As	Arsenic				
ASD	Analytical Spectral Devices				
ASTER	Advanced Spaceborne Thermal Emission and Reflection Radiometer				
<b>AVIRIS-NG</b>	Airborne Visible-Infrared Imaging Spectrometer-Next Generation				
AWTS	Area Wavelet Transform Stress Signal				
BP	Back Propagation				
BPNN	Back Propagation Neural Network				
CARS	Competitive Adaptive Reweighted Sampling				
Catboost	Categorical Boosting (a machine learning algorithm)				
Cd	Cadmium				
CIred-edge	Red-edge Chlorophyll Index				
Co	Cobalt				
Cr	Chromium				
CSVI	Copper Stress Vegetation Index				
Cu	Copper				
DWRT	Dry Weight of Roots				
ESA	European Space Agency				
EVI	Enhanced Vegetation Index				
Fe	Iron				
$Fe_2O_3$	Hematite				
GA	Genetic Algorithm				

Genetic Algorithm GΑ **Gradient Boosting Regression Tree GBRT** 

**GNDVI** Green Normalized Difference Vegetation Index

**GWR** Geographically Weighted Regression

**HCSI** Heavy Metal Cd Stress-Sensitive Spectral Index

Mercury Hg Heavy Metal HM

**HMSI** Normalized Heavy-Metal Stress Index **HMSSI** Heavy Metal Stress Sensitive Index

Remote Sens. **2024**, 16, 3221 21 of 30

KS Kolmogorov–Smirnov rank

LAI Leaf Area Index LARS Least Angle Regression

LASSO Least Absolute Shrinkage and Selection Operator

ML Machine Learning

MLR Multiple Linear Regression

MCARI Modified Chlorophyll Absorption Ratio Index

Mn Manganese

MTCI MERIS Terrestrial Chlorophyll Index

MSR Modified Simple Ratio

N Nitrogen

NDRE Normalized Difference Red-edge Index NDVI Normalized Difference Vegetation Index NDWI Normalized Difference Water Index

Ni Nickel

NIR Near Infrared Reflectance NSI Nitrogen Stress Index

NVI Normalized Chlorophyll Index NWI Normalized Water Index

OLS Ordinary Least Squares estimation method

PCR Principal Component Regression PLSR Partial Least Squares Regression

Pb Lead

PSRI Plant Senescence Reflectance Index

RCBP Radar Plots of Characteristic Band Pearson Coefficients

RDVI Renormalized Difference Vegetation Index

REP Red-edge Position

RFR Random Forest Regression
RPI Relative Phenophase Index

RS Remote Sensing

RVR Reference Vector Regression

Sn Stannum (Tin)

SIST Stress Index based on Spatial and Temporal Characteristics

SMLR Stepwise Multiple Linear Regression

SR Simple Ratio Index
SRWI Simple Ratio Water Index
SVI Stress vegetation Index
SWIR Shortwave Infrared

SWSI Salinity and Water Stress Index

TSA Time Series Analysis
UAS Unmanned Aerial System
VII Vegetation Inferiority Index

VIGS Vegetation Index considering Greenness and Shortwave Infrared

VNIR Visible Near-Infrared

WDI Water Absorption Disrelated Index

WOFOST World Food Study

Zn Zinc

Remote Sens. **2024**, 16, 3221 22 of 30

# Appendix A. Tables

**Table A1.** Proximal sensing studies for HM detection.

HM	Device	Important Wavelengths [nm]	Method	Reference
Al	ASD FieldSpec 3	480, 500, 565, 610, 680, 750, 1000, 1430, 1755, 1887, 1920, 1950, 2210, 2260	SMLR	[75]
	ASD FieldSpec 3	594, 990–991, 1185, 1447–1448, 1843–1844, 1865, 2237, 2301–2307	PLSR, MLR	[165]
As	ASD FieldSpec 3 ASD FieldSpec 4	402, 420, 566, 577, 689, 690, 697, 2382, 2393 622, 746, 930, 938, 1102, 1122, 1274	GBRT, CARS, SVR, LRM, RFR RCBP, Catboost	[166] [71]
Cd	ASD FieldSpec 3 ASD FieldSpec 3 ASD FieldSpec 3 ASD FieldSpec 3	1400, 1900, 2200 400–2400 681, 683, 693, 694, 699, 769–776, 880, 1018, 1461 594, 990–991, 1185, 1447–1448, 1843– 1844, 1865, 2237, 2301–2307	RFR, PCR, OBCA KS, OLS PLSR, MLR	[167] [69] [68] [165]
	FieldSpec FR PSR-3500 PSR-3500	1300–1450, 1850–1950, 2200–2400 400–2400 581–626, 670–690	PLSR PLSR, GA PLSR, BPNN	[84] [168] [78]
Cr	ASD FieldSpec 3 ASD FieldSpec 3 ASD FieldSpec 3 ASD FieldSpec 4	480, 500, 610, 715, 750, 860, 1300, 1430, 1755, 1920, 1950 400–2400 400–2400 600–800	SMLR PLSR KS, OLS PLSR, PCR, SVR	[75] [83] [69] [169]
Cu	ASD FieldSpec 3 ASD FieldSpec 3 ASD FieldSpec 4 ASD FieldSpec 4 FieldSpec FR	1925 400–2400 480, 500, 610, 750, 860, 1300, 1430, 1920, 2150, 2260 750, 860, 1300, 1430, 1920, 2150, 2260 390–1000	PLSR KS, OLS SMLR PLSR, BPNN PLSR	[170] [69] [75] [70] [84]
Fe	FieldSpec FR	390–550, 1300–1450, 1850–1950, 2200–2400	PLSR	[84]
Hg	AvaField	465, 799, 1373, 2114	MLR, BPNN, GA-BPNN	[171]
Mn	ASD FieldSpec 4	1318, 1646, 1806, 2271, 2275, 2383	RCBP, Catboost	[71]
Ni	ASD FieldSpec 3 ASD FieldSpec 4 PSR-3500	1393 600–800 600–800	PLSR PLSR, PCR, SVR PLSR	[170] [169] [172]
Pb	ASD FieldSpec 2 ASD FieldSpec 3 ASD FieldSpec 3	700–1400 594, 990–991, 1185, 1447–1448, 1843–1844, 1865, 2237, 2301–2307 400–2400	MLR, ANN PLSR, MLR KS, OLS	[25] [165] [69]
	ASD FieldSpec 3 ASD FieldSpec 4 ASD FieldSpec 4 Lambda900	712–713, 717–720, 727–728, 751–752, 757–758, 815, 1280, 1476, 1601 450–580, 730–760 450, 466, 622, 1278, 1530 838, 1930, 2148	PLSR, BPNN RCBP, Catboost PLSR, LARS	[68] [70] [71] [77]
Sn	ASD FieldSpec 4	1600–1800, 2000–2200	PLSR, BPNN	[70]
Zn	ASD FieldSpec 3 ASD FieldSpec 4 ASD FieldSpec 4 ASD FieldSpec 4 PSR-3500	400–2400 515 550 450, 622, 630, 1230 1400, 1900, 2200	KS, OLS PLSR PLSR, BPNN RCBP, Catboost PLSR, GA	[69] [173] [70] [71] [174]

Remote Sens. **2024**, 16, 3221 23 of 30

**Table A2.** Remote sensing studies for soil HM detection.

Imaging Type	Remote Sensor	НМ	Method	Reference
	Landsat 7	Cd, Co, Cr, Cu, Fe, Mn, Ni, Pb, Zn	NDVI, NDVI anomalies	[97]
	Landsat 7	As, Cd, Cr, Co, Cu, Hg, Mn, Ni, Pb, Sb	RFR, PLSR, SVR	[98]
	Landsat 8	As, Cu, Pb	GA-BP	[100]
TE.	Landsat 8	Cu, Pb	GA-BP	[101]
ij	Landsat 8	As, Cu, Hg	PLSR, ANN, RVR	[102]
ьĕ	Landsat 8	As, Cr, Cu, Pb, Ni, Zn	Cubist	[94]
tis	Landsat 8	As, Cd, Cr, Cu, Hg, Ni, Pb, Zn	Kriging and co-Kriging	[103]
Multispectral	Landsat 8	As, Cd, Cr, Cu, Hg, Ni, Pb, Zn	LASSO-GA-BPNN, SVR, RFR, Spat. Int.	[104]
	Landsat 8	Cr, Cu, Mn, Ni, V, Zn	SMLR, PLSR	[105]
	Landsat 8	Pb	RFR	[106]
	Landsat 8, ASTER, SPOT 5	Zn	RFR, GWR	[99]
	Landsat 8, Sentinel-2	As, Cr, Fe, Pb, Zn	GA, PLSR	[110]
	Sentinel-2	Cu, Ni, Pb	MLR, SMLR	[107]
	Sentinel-2	Cd, Pb	RFR, PLSR, BPNN	[108]
	НуМАР	As, Cu, Pb, Zn	MLR	[63]
	HyMAP	As, Pb	-	[111]
_	HyMAP-C	As, Cr, Pb, Zn	CARS-Stacking	[119,120]
Ţ,	HySpex VNIR	Cr, Cu, Ni, Zn	MLR	[112]
ec	Hyperion	As, Cd, Pb, Zn	PLSR	[113]
Hyperspectral	Hyperion, Geofen-5, Ziyuan-1, HyMap	Ni, Zn, Pb	GA, PLSR	[95]
Нуј	Geofen-5	Cu	GA, PLSR, Kriging	[114]
	UAS	Cu, Cr	GBRT	[115]
	UAS	As, Cd, Cr, Cu, Hg, Ni, Pb, Zn	BPNN, RFR	[116]

**Table A3.** Remote sensing studies for detecting HM impact on vegetation.

Remote Sensor	НМ	Vegetation Study Site	Indices	Method	Reference
Landsat MSS	Ni, Cu	Vegetation, Kola (Russia)	NDVI	TSA of NDVI and classification	[132]
Landsat 7	Cd, Co, Cr, Cu, Fe, Mn, Ni, Pb, Zn	Vegetation, Agri (Italy)	NDVI	Correlation	[97]
Landsat 7	Cu, Pb, Zn, and Cd	Vegetation, Sumatra (Indonesia)	VIGS	New index VIGS, correlation	[147]
Landsat 8	Cd, Hg, Pb	Rice, Hunan (China)	HMSI, GNDVI	Triangular model and HMSI	[148]
MODIS, Landsat 7 and Landsat 8	Cd	Rice, Hunan (China)	EVI	Stress signal AWTS	[175]
MODIS, Landsat	Cd	Xiangjiang Basin (China)	EVI, NDWI	Index phenology	[134]
MODIS, Landsat 8	Cd, Hg, Pb, As	Rice, Hunan (China)	NDVI and NDWI	New RPI index, NDVI and NDWI TSA	[176]
Sentinel-2	Cd, Hg, and Pb	Rice, Zhuzhou (China)	HMSSI, CIred-edge, PSRI	New index HMSSI	[135]
Sentinel-2	Cd	Rice, Zhuzhou (China)	HCSI	New index, PROSAIL	[149]
Sentinel-2	Cd	Rice, Zhuzhou (China)	-	New stress index SIST, LAI TSA	[139]
Sentinel-2	Cd	Rice, Zhuzhou (China)	REP, CIred-edge, MSR, MCARI, NDVI, RDVI, NDRE	GRU	[141]
Sentinel-2	Cd	Rice, Hunan (China)	NDRE	Bayesian statistics	[138]
Sentinel-2	Cd	Rice, Hunan (China)		FAPAR TSA	[92]
MODIS, Sentinel-2	-	Mining areas, Liaoning (China)	NDVI, MTCI	Long-term vegetation change, spatial chlorophyll change	[140]

Remote Sens. **2024**, 16, 3221 24 of 30

Table A3. Cont.

Remote Sensor	HM	Vegetation Study Site	Indices	Method	Reference
Headwall, Hyspex	Cu, Zn, As, Sn, Cr, Cd	Grassland, Xilinhot (China)	NDVI	RFR model inversion	[144]
HySpex	Cr, Cu, Ni, Zn	industrial brownfield	NDVI	Scaled relationship	[112]
AVIRIS-NG	-	Vegetation, Jharia (India)	NDVI, NSI, SR, SWSI, SRWI, NWI, CSVI, HMSSI, ARI	VI combination	[142]
HyMap, Hyperion	$Fe_2O_3$	Mining area, Australia and China	VII, WDI, NDVI	Index spatial variation	[133]
Hyperion	As and Pb	Eucalyptus, Bam (Iran)	-	Spectral angle mapper	[146]
Hyperion, Radarsat-2	Pb	Rice, Suzhou (China)	NVI, SVI	NVI-SVI feature space	[150]
Hyperion	Cu	Vegetation, Dexing (China)	CSVI	Correlation	[137]
НЈ-1	Cu	Vegetation, Dexing Mine (China)	-	Sensitive wavelength, extrapolated MLR	[143]
HJ-1A/B	Cd, Pb, As	Rice, Xiangjiang River (China)	EVI	Phenological changes, EVI TSA	[126]
HJ-1A/B, Landsat 7, Landsat 8	Cd	Rice, Hunan (China)	NDVI	NDVI, simulated DWRT by WOFOST	[136]
НЈ-1А	Cd, As	Farmland, Xushe (China)	-	Regression	[145]
Gaofen 5-02, Zhuhai-1 OHS-3D	Cu, Zn, Cd, and Pb	Maize, Majuan (China)	-	Domain adaptation	[151]

## References

- 1. Raffa, C.M.; Chiampo, F.; Shanthakumar, S. Remediation of Metal/Metalloid-Polluted Soils: A Short Review. *Appl. Sci.* **2021**, *11*, 4134. [CrossRef]
- 2. Mohammed, A.S.; Kapri, A.; Goel, R. Heavy Metal Pollution: Source, Impact, and Remedies. In *Biomanagement of Metal-Contaminated Soils*; Springer: Dordrecht, The Netherlands, 2011; pp. 1–28. [CrossRef]
- 3. Briffa, J.; Sinagra, E.; Blundell, R. Heavy metal pollution in the environment and their toxicological effects on humans. *Heliyon* **2020**, *6*, e04691. [CrossRef]
- 4. Edelstein, M.; Ben-Hur, M. Heavy metals and metalloids: Sources, risks and strategies to reduce their accumulation in horticultural crops. *Sci. Hortic.* **2018**, 234, 431–444. [CrossRef]
- 5. Uchimiya, M.; Bannon, D.; Nakanishi, H.; McBride, M.B.; Williams, M.A.; Yoshihara, T. Chemical Speciation, Plant Uptake, and Toxicity of Heavy Metals in Agricultural Soils. *J. Agric. Food Chem.* **2020**, *68*, 12856–12869. [CrossRef] [PubMed]
- 6. Cheng, S. Heavy metal pollution in China: Origin, pattern and control. Environ. Sci. Pollut. Res. 2003, 10, 192–198. [CrossRef]
- 7. Zhang, Q.; Wang, C. Natural and Human Factors Affect the Distribution of Soil Heavy Metal Pollution: A Review. *Water Air Soil Pollut*. **2020**, *231*, *350*. [CrossRef]
- 8. Jia, X.; O'Connor, D.; Shi, Z.; Hou, D. VIRS based detection in combination with machine learning for mapping soil pollution. *Environ. Pollut.* **2021**, 268, 115845. [CrossRef]
- 9. Shawai, S.A.A.; Muktar, H.I.; Bataiya, A.G.; Abdullahi, I.I.; Shamsuddin, I.M.; Yahaya, A.S.; Suleiman, M. A Review on Heavy Metals Contamination in Water and Soil: Effects, Sources and Phytoremediation Techniques. *Int. J. Miner. Process. Extr. Metall.* **2017**, 2, 21–27. [CrossRef]
- 10. Mitra, S.; Chakraborty, A.J.; Tareq, A.M.; Emran, T.B.; Nainu, F.; Khusro, A.; Idris, A.M.; Khandaker, M.U.; Osman, H.; Alhumaydhi, F.A.; et al. Impact of heavy metals on the environment and human health: Novel therapeutic insights to counter the toxicity. *J. King Saud Univ.-Sci.* 2022, 34, 101865. [CrossRef]
- 11. Sager, M.; Wiche, O. Rare Earth Elements (REE): Origins, Dispersion, and Environmental Implications—A Comprehensive Review. *Environments* **2024**, *11*, 24. [CrossRef]
- 12. Pourret, O.; Hursthouse, A. It's Time to Replace the Term "Heavy Metals" with "Potentially Toxic Elements" When Reporting Environmental Research. *Int. J. Environ. Res. Public Health* **2019**, *16*, 4446. [CrossRef] [PubMed]
- 13. Rizvi, A.; Zaidi, A.; Ameen, F.; Ahmed, B.; AlKahtani, M.D.F.; Khan, M.S. Heavy metal induced stress on wheat: Phytotoxicity and microbiological management. *RSC Adv.* **2020**, *10*, 38379–38403. [CrossRef] [PubMed]
- 14. Marschner, H. 1-Introduction, Definition, and Classification of Mineral Nutrients. In *Marschner's Mineral Nutrition of Higher Plants*, 2nd ed.; Marschner, H., Ed.; Academic Press: San Diego, CA, USA, 2002; pp. 3–5. [CrossRef]

Remote Sens. **2024**, 16, 3221 25 of 30

15. Tóth, G.; Hermann, T.; Szatmári, G.; Pásztor, L. Maps of heavy metals in the soils of the European Union and proposed priority areas for detailed assessment. *Sci. Total Environ.* **2016**, *565*, 1054–1062. [CrossRef] [PubMed]

- 16. Marini, M.; Caro, D.; Thomsen, M. The new fertilizer regulation: A starting point for cadmium control in European arable soils? *Sci. Total Environ.* **2020**, 745, 140876. [CrossRef] [PubMed]
- 17. Fuentes-Arderiu, X. Concentration and content. Biochem. Med. 2013, 23, 141–142. [CrossRef]
- 18. Alloway, B.J. *Heavy Metals in Soils: Trace Metals and Metalloids in Soils and Their Bioavailability;* Springer: Dordrecht, The Netherlands, 2013. [CrossRef]
- 19. Seibold, E.; Berger, W.H. The Sea Floor: An Introduction to Marine Geology; Springer: Cham, Switzerland, 1993; p. 356.
- 20. Orhue, E.R.; Frank, U.O. Fate of some heavy metals in soils: A review. J. Appl. Nat. Sci. 2011, 3, 131–138. [CrossRef]
- 21. Uchimiya, M. Influence of pH, Ionic Strength, and Multidentate Ligand on the Interaction of CdII with Biochars. *ACS Sustain. Chem. Eng.* **2014**, *2*, 2019–2027. [CrossRef]
- 22. Gadd, G.M. Geomycology: Biogeochemical transformations of rocks, minerals, metals and radionuclides by fungi, bioweathering and bioremediation. *Mycol. Res.* **2007**, *111*, 3–49. [CrossRef]
- 23. Uchimiya, M.; Stone, A.T. Reversible redox chemistry of quinones: Impact on biogeochemical cycles. *Chemosphere* **2009**, 77, 451–458. [CrossRef]
- 24. Francos, N.; Gholizadeh, A.; Ben Dor, E. Spatial distribution of lead (Pb) in soil: A case study in a contaminated area of the Czech Republic. *Geomat. Nat. Hazards Risk* **2022**, *13*, 610–620. [CrossRef]
- 25. Kemper, T.; Sommer, S. Estimate of Heavy Metal Contamination in Soils after a Mining Accident Using Reflectance Spectroscopy. *Environ. Sci. Technol.* **2002**, *36*, 2742–2747. [CrossRef] [PubMed]
- 26. Xu, R.; Zhang, M.; Lin, H.; Gao, P.; Yang, Z.; Wang, D.; Sun, X.; Li, B.; Wang, Q.; Sun, W. Response of soil protozoa to acid mine drainage in a contaminated terrace. *J. Hazard. Mater.* **2022**, 421, 126790. [CrossRef] [PubMed]
- 27. Liu, Y.R.; Delgado-Baquerizo, M.; Bi, L.; Zhu, J.; He, J.Z. Consistent responses of soil microbial taxonomic and functional attributes to mercury pollution across China. *Microbiome* **2018**, *6*, 183. [CrossRef]
- 28. Enya, O.; Heaney, N.; Iniama, G.; Lin, C. Effects of heavy metals on organic matter decomposition in inundated soils: Microcosm experiment and field examination. *Sci. Total Environ.* **2020**, 724, 138223. [CrossRef]
- 29. Šantručková, H.; Krištufková, M.; Vaněk, D. Decomposition rate and nutrient release from plant litter of Norway spruce forest in the Bohemian Forest. *Biologia* **2006**, *61*, S499–S508. [CrossRef]
- 30. Arif, N.; Yadav, V.; Singh, S.; Singh, S.; Ahmad, P.; Mishra, R.K.; Sharma, S.; Tripathi, D.K.; Dubey, N.K.; Chauhan, D.K. Influence of High and Low Levels of Plant-Beneficial Heavy Metal Ions on Plant Growth and Development. *Front. Environ. Sci.* **2016**, *4*, 69. [CrossRef]
- 31. Kumchai, J.; Huang, J.; Lee, C.; Chen, F.; Chin, S. Proline partially overcomes excess molybdenum toxicity in cabbage seedlings grown in vitro. *Genet. Mol. Res.* **2013**, 12, 5589–5601. [CrossRef] [PubMed]
- 32. Rout, G.R.; Das, P. Effect of metal toxicity on plant growth and metabolism: I. Zinc. Agronomie 2009, 32, 873–884.
- 33. Balestrasse, K.B.; Benavides, M.P.; Gallego, S.M.; Tomaro, M.L. Effect of cadmium stress on nitrogen metabolism in nodules and roots of soybean plants. *Funct. Plant Biol.* **2003**, *30*, 57–64. [CrossRef]
- 34. Sperdouli, I. Heavy Metal Toxicity Effects on Plants. Toxics 2022, 10, 715. [CrossRef] [PubMed]
- 35. Gajewska, E.; Skłodowska, M.; Słaba, M.; Mazur, J. Effect of nickel on antioxidative enzyme activities, proline and chlorophyll contents in wheat shoots. *Biol. Plant.* **2006**, *50*, 653–659. [CrossRef]
- 36. Yadav, N.; Maurya, B.M.; Chettri, D.; Pooja; Pulwani, C.; Jajula, M.; kanda, S.S.; babu, H.W.S.; Elangovan, A.; Velusamy, P.; et al. Artificial intelligence in heavy metals detection: Methodological and ethical challenges. *Hyg. Environ. Health Adv.* **2023**, 7, 100071. [CrossRef]
- 37. Sandrin, T.R.; Maier, R.M. Impact of metals on the biodegradation of organic pollutants. *Environ. Health Perspect.* **2003**, 111, 1093–1101. [CrossRef] [PubMed]
- 38. Jócsák, I.; Knolmajer, B.; Szarvas, M.; Rabnecz, G.; Pál-Fám, F. Literature Review on the Effects of Heavy Metal Stress and Alleviating Possibilities through Exogenously Applied Agents in Alfalfa (*Medicago sativa* L.). *Plants* **2022**, *11*, 2161. [CrossRef]
- 39. Shahzad, A.; Siddique, A.; Ferdous, S.; Amin, M.A.; Qin, M.; Aslam, U.; Naeem, M.; Bashir, T.; Shakoor, A. Heavy metals mitigation and growth promoting effect of endophytic *Agrococcus terreus* (MW 979614) in maize plants under zinc and nickel contaminated soil. *Front. Microbiol.* **2023**, *14*, 1255921. [CrossRef]
- 40. Sethy, S.K.; Ghosh, S. Effect of heavy metals on germination of seeds. J. Nat. Sci. Biol. Med. 2013, 4, 272–275. [CrossRef]
- 41. Jayakumar, K.; Jaleel, C.; Azooz, M. Impact of Cobalt on Germination and Seedling Growth of *Eleusine coracana* L. And Oryza sativa L. Under Hydroponic Culture. *Glob. J. Mol. Sci.* **2008**, *3*, 18–20.
- 42. Gang, A.; Vyas, A.; Vyas, H. Toxic effect of heavy metals on germination and seedling growth of wheat. *J. Environ. Res. Dev.* **2013**, *8*, 206–213.
- 43. Gwóźdź, E.A.; Przymusiński, R.; Rucińska, R.; Deckert, J. Plant cell responses to heavy metals: Molecular and physiological aspects. *Acta Physiol. Plant.* **1997**, *19*, 459–465. [CrossRef]
- 44. Sharma, S.S.; Dietz, K.J. The relationship between metal toxicity and cellular redox imbalance. *Trends Plant Sci.* **2009**, *14*, 43–50. [CrossRef]

Remote Sens. **2024**, 16, 3221 26 of 30

45. Krupa, Z.; Siedlecka, A.; Skórzynska-Polit, E.; Maksymiec, W. Heavy metal interactions with plant nutrients. In *Physiology and Biochemistry of Metal Toxicity and Tolerance in Plants*; Prasad, M.N.V., Strzałka, K., Eds.; Springer: Dordrecht, The Netherlands, 2002; pp. 287–301.

- 46. Alcántara, E.; Romera, F.J.; Cañete, M.; De La Guardia, M.D. Effects of heavy metals on both induction and function of root fe(lll) reductase in fe-deficient cucumber (*Cucumis sativus* L.) plants. *J. Exp. Bot.* **1994**, 45, 1893–1898. [CrossRef]
- 47. Marschner, H. Mineral Nutrition of Higher Plants; Academic Press: London, UK, 1986.
- 48. Ali, B.; Gill, R.A. Editorial: Heavy metal toxicity in plants: Recent insights on physiological and molecular aspects, volume II. *Front. Plant Sci.* **2022**, *13*, 1016257. [CrossRef] [PubMed]
- 49. Lee, C.W.; Choi, J.M.; Pak, C.H. Micronutrient Toxicity in Seed Geranium (Pelargonium × hortorum Bailey). *J. Am. Soc. Hortic. Sci.* **1996**, *121*, 77–82. [CrossRef]
- 50. Pandey, N.; Sharma, C.P. Effect of heavy metals Co<sup>2+</sup>, Ni<sup>2+</sup> and Cd<sup>2+</sup> on growth and metabolism of cabbage. *Plant Sci.* **2002**, 163, 753–758. [CrossRef]
- 51. Kopačková, V.; Lhotáková, Z.; Oulehle, F.; Albrechtová, J. Assessing forest health via linking the geochemical properties of a soil profile with the biochemical parameters of vegetation. *Int. J. Environ. Sci. Technol.* **2015**, *12*, 1987–2002. [CrossRef]
- 52. Baker, A.J. Accumulators and excluders-strategies in the response of plants to heavy metals. *J. Plant Nutr.* **1981**, *3*, 643–654. [CrossRef]
- 53. Ernst, W.H. Evolution of metal tolerance in higher plants. Snow Landsc. Res. 2006, 80, 251-274.
- 54. Colzi, I.; Rocchi, S.; Rangoni, M.; Del Bubba, M.; Gonnelli, C. Specificity of metal tolerance and use of excluder metallophytes for the phytostabilization of metal polluted soils: The case of *Silene paradoxa* L. *Environ. Sci. Pollut. Res.* **2014**, 21, 10960–10969. [CrossRef]
- 55. Noor, I.; Sohail, H.; Sun, J.; Nawaz, M.A.; Li, G.; Hasanuzzaman, M.; Liu, J. Heavy metal and metalloid toxicity in horticultural plants: Tolerance mechanism and remediation strategies. *Chemosphere* **2022**, *303*, 135196. [CrossRef]
- 56. Brooks, R.; Radford, C. Nickel accumulation by European species of the genus Alyssum. *Proc. R. Soc. Lond. Ser. B. Biol. Sci.* **1978**, 200, 217–224.
- 57. Van der Ent, A.; Baker, A.J.; Reeves, R.D.; Pollard, A.J.; Schat, H. Hyperaccumulators of metal and metalloid trace elements: Facts and fiction. *Plant Soil* **2013**, *362*, 319–334. [CrossRef]
- 58. Riyazuddin, R.; Nisha, N.; Ejaz, B.; Khan, M.I.R.; Kumar, M.; Ramteke, P.W.; Gupta, R. A Comprehensive Review on the Heavy Metal Toxicity and Sequestration in Plants. *Biomolecules* **2022**, *12*, 43. [CrossRef] [PubMed]
- 59. Lwalaba, J.L.W.; Zvobgo, G.; Mwamba, T.M.; Louis, L.T.; Fu, L.; Kirika, B.A.; Tshibangu, A.K.; Adil, M.F.; Sehar, S.; Mukobo, R.P.; et al. High accumulation of phenolics and amino acids confers tolerance to the combined stress of cobalt and copper in barley (*Hordeum vulagare*). *Plant Physiol. Biochem.* **2020**, 155, 927–937. [CrossRef]
- Vasilachi, I.C.; Stoleru, V.; Gavrilescu, M. Analysis of Heavy Metal Impacts on Cereal Crop Growth and Development in Contaminated Soils. Agriculture 2023, 13, 1983. [CrossRef]
- 61. Salminen, R. Geochemical atlas of the eastern Barents region. J. Geochem. Explor. 2004, 83, 1–530.
- 62. Wei, L.F.; Zhang, Y.X.; Lu, Q.K.; Yuan, Z.R.; Li, H.B.; Huang, Q.B. Estimating the spatial distribution of soil total arsenic in the suspected contaminated area using UAV-Borne hyperspectral imagery and deep learning. *Ecol. Indic.* **2021**, *133*, 108384. [CrossRef]
- 63. Choe, E.; van der Meer, F.; van Ruitenbeek, F.; van der Werff, H.; de Smeth, B.; Kim, K.W. Mapping of heavy metal pollution in stream sediments using combined geochemistry, field spectroscopy, and hyperspectral remote sensing: A case study of the Rodalquilar mining area, SE Spain. *Remote Sens. Environ.* 2008, 112, 3222–3233. [CrossRef]
- 64. Ning, Y.; Li, J.; Cai, W.; Shao, X. Simultaneous determination of heavy metal ions in water using near-infrared spectroscopy with preconcentration by nano-hydroxyapatite. *Spectrochim. Acta Part A Mol. Biomol. Spectrosc.* **2012**, *96*, 289–294. [CrossRef] [PubMed]
- 65. Shi, T.; Chen, Y.; Liu, Y.; Wu, G. Visible and near-infrared reflectance spectroscopy—An alternative for monitoring soil contamination by heavy metals. *J. Hazard. Mater.* **2014**, 265, 166–176. [CrossRef]
- 66. Cheng, H.; Shen, R.; Chen, Y.; Wan, Q.; Shi, T.; Wang, J.; Wan, Y.; Hong, Y.; Li, X. Estimating heavy metal concentrations in suburban soils with reflectance spectroscopy. *Geoderma* **2019**, *336*, 59–67. [CrossRef]
- 67. Kästner, F.; Sut-Lohmann, M.; Ramezany, S.; Raab, T.; Feilhauer, H.; Chabrillat, S. Estimating heavy metal concentrations in Technosols with reflectance spectroscopy. *Geoderma* **2022**, *406*, 115512. [CrossRef]
- 68. Zhang, S.; Li, J.; Wang, S.; Huang, Y.; Li, Y.; Chen, Y.; Fei, T. Rapid Identification and Prediction of Cadmium-Lead Cross-Stress of Different Stress Levels in Rice Canopy Based on Visible and Near-Infrared Spectroscopy. *Remote Sens.* **2020**, *12*, 469. [CrossRef]
- 69. Zhang, Q.; Zhang, H.; Liu, W.; Zhao, S. Inversion of heavy metals content with hyperspectral reflectance in soil of well-facilitied capital farmland construction areas. *Trans. Chin. Soc. Agric. Eng.* **2017**, 33, 230–239.
- 70. Bian, Z.; Sun, L.; Tian, K.; Liu, B.; Zhang, X.; Mao, Z.; Huang, B.; Wu, L. Estimation of Heavy Metals in Tailings and Soils Using Hyperspectral Technology: A Case Study in a Tin-Polymetallic Mining Area. *Bull. Environ. Contam. Toxicol.* **2021**, 107, 1022–1031. [CrossRef] [PubMed]
- 71. Fu, P.; Zhang, J.; Yuan, Z.; Feng, J.; Zhang, Y.; Meng, F.; Zhou, S. Estimating the Heavy Metal Contents in Entisols from a Mining Area Based on Improved Spectral Indices and Catboost. *Sensors* **2024**, *24*, 1492. [CrossRef]
- 72. Malik, L.A.; Bashir, A.; Qureashi, A.; Pandith, A.H. Detection and removal of heavy metal ions: A review. *Environ. Chem. Lett.* **2019**, *17*, 1495–1521. [CrossRef]

Remote Sens. **2024**, 16, 3221 27 of 30

73. Wang, F.; Gao, J.; Zha, Y. Hyperspectral sensing of heavy metals in soil and vegetation: Feasibility and challenges. *ISPRS J. Photogramm. Remote Sens.* **2018**, 136, 73–84. [CrossRef]

- 74. Baveye, P.C.; Laba, M. Visible and near-infrared reflectance spectroscopy is of limited practical use to monitor soil contamination by heavy metals. *J. Hazard. Mater.* **2015**, *285*, 137–139. [CrossRef] [PubMed]
- 75. Song, L.; Jian, J.; Tan, D.J.; Xie, H.B.; Luo, Z.F.; Gao, B. Estimate of heavy metals in soil and streams using combined geochemistry and field spectroscopy in Wan-sheng mining area, Chongqing, China. *Int. J. Appl. Earth Obs. Geoinf.* **2015**, 34, 1–9. [CrossRef]
- 76. Omran, E.S.E. Inference model to predict heavy metals of Bahr El Baqar soils, Egypt using spectroscopy and chemometrics technique. *Model. Earth Syst. Environ.* **2016**, 2, 1–17. [CrossRef]
- 77. Zhang, X.; Wen, J.; Zhao, D. Band selection method for retrieving soil lead content with hyperspectral remote sensing data. In Proceedings of the SPIE Remote Sensing, Toulouse, France, 20–23 September 2010; Volume 7831, p. 78311K. [CrossRef]
- 78. Chen, T.; Chang, Q.; Clevers, J.; Kooistra, L. Rapid identification of soil cadmium pollution risk at regional scale based on visible and near-infrared spectroscopy. *Environ. Pollut.* **2015**, *206*, 217–226. [CrossRef] [PubMed]
- 79. Song, Y.; Li, F.; Yang, Z.; Ayoko, G.A.; Frost, R.L.; Ji, J. Diffuse reflectance spectroscopy for monitoring potentially toxic elements in the agricultural soils of Changjiang River Delta, China. *Appl. Clay Sci.* **2012**, *64*, 75–83. [CrossRef]
- 80. Wang, J.; Cui, L.; Gao, W.; Shi, T.; Chen, Y.; Gao, Y. Prediction of low heavy metal concentrations in agricultural soils using visible and near-infrared reflectance spectroscopy. *Geoderma* **2014**, *216*, 1–9. [CrossRef]
- 81. Zhao, D.; Wang, J.; Jiang, X.; Zhen, J.; Miao, J.; Wang, J.; Wu, G. Reflectance spectroscopy for assessing heavy metal pollution indices in mangrove sediments using XGBoost method and physicochemical properties. *Catena* **2022**, 211, 105967. [CrossRef]
- 82. Luce, M.S.; Ziadi, N.; Gagnon, B.; Karam, A. Visible near infrared reflectance spectroscopy prediction of soil heavy metal concentrations in paper mill biosolid-and liming by-product-amended agricultural soils. *Geoderma* **2017**, 288, 23–36. [CrossRef]
- 83. Wang, J.; Hu, X.; Shi, T.; He, L.; Hu, W.; Wu, G. Assessing toxic metal chromium in the soil in coal mining areas via proximal sensing: Prerequisites for land rehabilitation and sustainable development. *Geoderma* **2022**, 405, 115399. [CrossRef]
- 84. Xie, X.L.; Pan, X.Z.; Sun, B. Visible and Near-Infrared Diffuse Reflectance Spectroscopy for Prediction of Soil Properties near a Copper Smelter. *Pedosphere* **2012**, 22, 351–366. [CrossRef]
- 85. Yu, K.; Van Geel, M.; Ceulemans, T.; Geerts, W.; Ramos, M.M.; Serafim, C.; Sousa, N.; Castro, P.M.L.; Kastendeuch, P.; Najjar, G.; et al. Vegetation reflectance spectroscopy for biomonitoring of heavy metal pollution in urban soils. *Environ. Pollut.* **2018**, 243, 1912–1922. [CrossRef]
- 86. Liu, M.; Liu, X.; Li, J.; Li, T. Estimating regional heavy metal concentrations in rice by scaling up a field-scale heavy metal assessment model. *Int. J. Appl. Earth Obs. Geoinf.* **2012**, *19*, 12–23. [CrossRef]
- 87. Li, Y.; Yang, K.; Cheng, F.; Zhang, C. Development of a new heavy metal vegetation index for improving monitoring of copper and lead concentration in corn. *Eur. J. Remote Sens.* **2019**, *52*, 632–639. [CrossRef]
- 88. Kanke, Y.; Tubaña, B.; Dalen, M.; Harrell, D. Evaluation of red and red-edge reflectance-based vegetation indices for rice biomass and grain yield prediction models in paddy fields. *Precis. Agric.* **2016**, *17*, 507–530. [CrossRef]
- 89. Maliki, A.A.; Owens, G.; Bruce, D. Capabilities of remote sensing hyperspectral images for detection of lead contamination: A review. *ISPRS Ann. Photogramm. Remote. Sens. Spat. Inf. Sci.* **2012**, *I-7*, 55–60. [CrossRef]
- 90. Horta, A.; Malone, B.; Stockmann, U.; Minasny, B.; Bishop, T.; McBratney, A.; Pallasser, R.; Pozza, L. Potential of integrated field spectroscopy and spatial analysis for enhanced assessment of soil contamination: A prospective review. *Geoderma* **2015**, 241–242, 180–209. [CrossRef]
- 91. Riedel, F.; Denk, M.; Müller, I.; Barth, N.; Gläßer, C. Prediction of soil parameters using the spectral range between 350 and 15,000 nm: A case study based on the Permanent Soil Monitoring Program in Saxony, Germany. *Geoderma* 2018, 315, 188–198. [CrossRef]
- 92. Li, M.; Liu, M.; Liu, X.; Peng, T.; Wang, S. Decomposition of long time-series fraction of absorbed photosynthetically active radiation signal for distinguishing heavy metal stress in rice. *Comput. Electron. Agric.* **2022**, *198*, 107111. [CrossRef]
- 93. Wei, X.; Liu, Y.; Shen, L.; Lu, Z.; Ai, Y.; Wang, X. Machine learning insights in predicting heavy metals interaction with biochar. *Biochar* **2024**, *6*, 10. [CrossRef]
- 94. Peng, Y.; Kheir, R.B.; Adhikari, K.; Malinowski, R.; Greve, M.B.; Knadel, M.; Greve, M.H. Digital Mapping of Toxic Metals in Qatari Soils Using Remote Sensing and Ancillary Data. *Remote Sens.* **2016**, *8*, 1003. [CrossRef]
- 95. Wang, Y.; Zhang, X.; Sun, W.; Wang, J.; Ding, S.; Liu, S. Effects of hyperspectral data with different spectral resolutions on the estimation of soil heavy metal content: From ground-based and airborne data to satellite-simulated data. *Sci. Total Environ.* **2022**, 838, 156129. [CrossRef] [PubMed]
- 96. Shi, T.; Guo, L.; Chen, Y.; Wang, W.; Shi, Z.; Li, Q.; Wu, G. Proximal and remote sensing techniques for mapping of soil contamination with heavy metals. *Appl. Spectrosc. Rev.* **2018**, *53*, 783–805. [CrossRef]
- 97. D'Emilio, M.; Macchiato, M.; Ragosta, M.; Simoniello, T. A method for the integration of satellite vegetation activities observations and magnetic susceptibility measurements for monitoring heavy metals in soil. *J. Hazard. Mater.* **2012**, 241–242, 118–126. [CrossRef]
- 98. Mouazen, A.M.; Nyarko, F.; Qaswar, M.; Tóth, G.; Gobin, A.; Moshou, D. Spatiotemporal Prediction and Mapping of Heavy Metals at Regional Scale Using Regression Methods and Landsat 7. *Remote Sens.* **2021**, *13*, 4615. [CrossRef]
- 99. Shi, T.; Hu, X.; Guo, L.; Su, F.; Tu, W.; Hu, Z.; Liu, H.; Yang, C.; Wang, J.; Zhang, J.; et al. Digital mapping of zinc in urban topsoil using multisource geospatial data and random forest. *Sci. Total Environ.* **2021**, 792, 148455. [CrossRef]

Remote Sens. **2024**, 16, 3221 28 of 30

100. Yang, Y.; Cui, Q.; Jia, P.; Liu, J.; Bai, H. Estimating the heavy metal concentrations in topsoil in the Daxigou mining area, China, using multispectral satellite imagery. *Sci. Rep.* **2021**, *11*, 11718. [CrossRef] [PubMed]

- 101. Yang, Y.; Cui, Q.; Cheng, R.; Huo, A.; Wang, Y. Retrieval of Soil Heavy Metal Content for Environment Monitoring in Mining Area via Transfer Learning. *Sustainability* **2023**, *15*, 11765. [CrossRef]
- 102. Fang, Y.; Xu, L.; Peng, J.; Wang, H.; Wong, A.; Clausi, D.A. Retrieval and mapping of heavy metal concentration in soil using time series Landsat 8 imagery. *Int. Arch. Photogramm. Remote. Sens. Spat. Inf. Sci.* **2018**, XLII-3, 335–340. [CrossRef]
- 103. Zeng, L.; Wang, Y.; Jing, L.; Cheng, Q. Quantitative determination of auxiliary information for mapping soil heavy metals and soil contamination risk assessment. *Appl. Geochem.* **2021**, *130*, 104964. [CrossRef]
- 104. Shi, S.; Hou, M.; Gu, Z.; Jiang, C.; Zhang, W.; Hou, M.; Li, C.; Xi, Z. Estimation of Heavy Metal Content in Soil Based on Machine Learning Models. *Land* 2022, *11*, 1037. [CrossRef]
- 105. Guan, Q.; Zhao, R.; Wang, F.; Pan, N.; Yang, L.; Song, N.; Xu, C.; Lin, J. Prediction of heavy metals in soils of an arid area based on multi-spectral data. *J. Environ. Manag.* **2019**, 243, 137–143. [CrossRef]
- 106. Xu, X.; Wang, Z.; Song, X.; Zhan, W.; Yang, S. A remote sensing-based strategy for mapping potentially toxic elements of soils: Temporal-spatial-spectral covariates combined with random forest. *Environ. Res.* **2024**, 240, 117570. [CrossRef]
- 107. Mirzaei, F.; Abbasi, Y.; Sohrabi, T. Modeling the distribution of heavy metals in lands irrigated by wastewater using satellite images of Sentinel-2. *Egypt. J. Remote Sens. Space Sci.* **2021**, 24, 537–546. [CrossRef]
- 108. Wang, L.; Zhou, Y.; Liu, J.; Liu, Y.; Zuo, Q.; Li, Q. Exploring the potential of multispectral satellite images for estimating the contents of cadmium and lead in cropland: The effect of the dimidiate pixel model and random forest. *J. Clean. Prod.* **2022**, 367, 132922. [CrossRef]
- 109. Beygi, S.; Talovina, I.V.; Tadayon, M.; Beiranvand Pour, A. Alteration and structural features mapping in Kacho-Mesqal zone, Central Iran using ASTER remote sensing data for porphyry copper exploration. *Int. J. Image Data Fusion* **2021**, *12*, 155–175. [CrossRef]
- 110. Khosravi, V.; Gholizadeh, A.; Saberioon, M. Soil toxic elements determination using integration of Sentinel-2 and Landsat-8 images: Effect of fusion techniques on model performance. *Environ. Pollut.* **2022**, *310*, 119828. [CrossRef] [PubMed]
- 111. Kemper, T.; Sommer, S. Use of airborne hyperspectral data to estimate residual heavy metal contamination and acidification potential in the Guadiamar floodplain Andalusia, Spain after the Aznacollar mining accident. In Proceedings of the International Society for Optics and Photonics, Remote Sensing, Canary Islands, Spain, 13–16 September 2004; Volume 5574, pp. 224–234. [CrossRef]
- 112. Lassalle, G.; Fabre, S.; Credoz, A.; Hédacq, R.; Dubucq, D.; Elger, A. Mapping leaf metal content over industrial brownfields using airborne hyperspectral imaging and optimized vegetation indices. *Sci. Rep.* **2021**, *11*, 2. [CrossRef]
- 113. Yang, L.Y.; Gao, X.H.; Zhang, W.; Shi, F.F.; He, L.H.; Jia, W. Estimating heavy metal concentrations in topsoil from vegetation reflectance spectra of Hyperion images: A case study of Yushu County, Qinghai, China. *Chin. J. Appl. Ecol.* 2016, 27, 1775–1784. [CrossRef]
- 114. Sun, W.; Liu, S.; Wang, M.; Zhang, X.; Shang, K.; Liu, Q. Soil copper concentration map in mining area generated from AHSI remote sensing imagery. *Sci. Total Environ.* **2023**, *860*, 160511. [CrossRef] [PubMed]
- 115. Gan, W.; Zhang, Y.; Xu, J.; Yang, R.; Xiao, A.; Hu, X. Spatial Distribution of Soil Heavy Metal Concentrations in Road-Neighboring Areas Using UAV-Based Hyperspectral Remote Sensing and GIS Technology. *Sustainability* **2023**, *15*, 10043. [CrossRef]
- 116. Chen, H.W.; Chen, C.Y.; Nguyen, K.L.P.; Chen, B.J.; Tsai, C.H. Hyperspectral sensing of heavy metals in soil by integrating AI and UAV technology. *Environ. Monit. Assess.* **2022**, *194*, 518. [CrossRef]
- 117. Chen, Q.; Zhao, Z.; Zhou, J.; Zhu, R.; Xia, J.; Sun, T.; Zhao, X.; Chao, J. ASTER and GF-5 Satellite Data for Mapping Hydrothermal Alteration Minerals in the Longtoushan Pb-Zn Deposit, SW China. *Remote Sens.* **2022**, *14*, 1253. [CrossRef]
- 118. Wang, Y.; Zou, B.; Chai, L.; Lin, Z.; Feng, H.; Tang, Y.; Tian, R.; Tu, Y.; Zhang, B.; Zou, H. Monitoring of soil heavy metals based on hyperspectral remote sensing: A review. *Earth-Sci. Rev.* **2024**, 254, 104814. [CrossRef]
- 119. Tan, K.; Wang, H.M.; Chen, L.H.; Du, Q.; Du, P.J.; Pan, C.C. Estimation of the spatial distribution of heavy metal in agricultural soils using airborne hyperspectral imaging and random forest. *J. Hazard. Mater.* **2020**, *382*, 13. [CrossRef] [PubMed]
- 120. Tan, K.; Ma, W.; Chen, L.; Wang, H.; Du, Q.; Du, P.; Yan, B.; Liu, R.; Li, H. Estimating the distribution trend of soil heavy metals in mining area from HyMap airborne hyperspectral imagery based on ensemble learning. *J. Hazard. Mater.* **2021**, 401, 123288. [CrossRef] [PubMed]
- 121. Song, W.; Song, W.; Gu, H.; Li, F. Progress in the Remote Sensing Monitoring of the Ecological Environment in Mining Areas. *Int. J. Environ. Res. Public Health* **2020**, *17*, 1846. [CrossRef] [PubMed]
- 122. Xie, M.; Li, H.; Zhu, Y.; Xue, J.; You, Q.; Jin, B.; Shi, Z. Predicting Bioaccumulation of Potentially Toxic Element in Soil–Rice Systems Using Multi-Source Data and Machine Learning Methods: A Case Study of an Industrial City in Southeast China. *Land* **2021**, *10*, 558. [CrossRef]
- 123. Chen, Y.; Liu, Y.; Liu, Y.; Liu, A.; Kong, X.; Liu, D.; Li, X.; Zhang, Y.; Gao, Y.; Wang, D. Mapping of Cu and Pb Contaminations in Soil Using Combined Geochemistry, Topography, and Remote Sensing: A Case Study in the Le'an River Floodplain, China. *Int. J. Environ. Res. Public Health* 2012, 9, 1874–1886. [CrossRef]
- 124. Moradpour, H.; Rostami Paydar, G.; Pour, A.B.; Valizadeh Kamran, K.; Feizizadeh, B.; Muslim, A.M.; Hossain, M.S. Landsat-7 and ASTER remote sensing satellite imagery for identification of iron skarn mineralization in metamorphic regions. *Geocarto Int.* **2022**, *37*, 1971–1998. [CrossRef]

Remote Sens. **2024**, 16, 3221

125. Diek, S.; Schaepman, M.E.; De Jong, R. Creating Multi-Temporal Composites of Airborne Imaging Spectroscopy Data in Support of Digital Soil Mapping. *Remote Sens.* **2016**, *8*, 906. [CrossRef]

- 126. Liu, S.; Liu, X.; Liu, M.; Wu, L.; Ding, C.; Huang, Z. Extraction of Rice Phenological Differences under Heavy Metal Stress Using EVI Time-Series from HJ-1A/B Data. *Sensors* **2017**, *17*, 1243. [CrossRef] [PubMed]
- 127. Gholizadeh, A.; Kopačková, V. Detecting vegetation stress as a soil contamination proxy: A review of optical proximal and remote sensing techniques. *Int. J. Environ. Sci. Technol.* **2019**, *16*, 2511–2524. [CrossRef]
- 128. Rai, P.K.; Lee, S.S.; Zhang, M.; Tsang, Y.F.; Kim, K.H. Heavy metals in food crops: Health risks, fate, mechanisms, and management. *Environ. Int.* **2019**, 125, 365–385. [CrossRef]
- 129. Bayat, B.; Van der Tol, C.; Verhoef, W. Remote Sensing of Grass Response to Drought Stress Using Spectroscopic Techniques and Canopy Reflectance Model Inversion. *Remote Sens.* **2016**, *8*, 557. [CrossRef]
- 130. Mirzaei, M.; Verrelst, J.; Marofi, S.; Abbasi, M.; Azadi, H. Eco-Friendly Estimation of Heavy Metal Contents in Grapevine Foliage Using In-Field Hyperspectral Data and Multivariate Analysis. *Remote Sens.* **2019**, *11*, 2731. [CrossRef] [PubMed]
- 131. Li, X.; Liu, X.; Liu, M.; Wang, C.; Xia, X. A hyperspectral index sensitive to subtle changes in the canopy chlorophyll content under arsenic stress. *Int. J. Appl. Earth Obs. Geoinf.* **2015**, *36*, 41–53. [CrossRef]
- 132. Mikkola, K. A remote sensing analysis of vegetation damage around metal smelters in the Kola Peninsula, Russia. *Int. J. Remote Sens.* **1996**, *17*, 3675–3690. [CrossRef]
- 133. Zhang, B.; Wu, D.; Zhang, L.; Jiao, Q.; Li, Q. Application of hyperspectral remote sensing for environment monitoring in mining areas. *Environ. Earth Sci.* 2012, 65, 649–658. [CrossRef]
- 134. Zou, X.; Liu, X.; Liu, M.; Liu, M.; Zhang, B. A Framework for Rice Heavy Metal Stress Monitoring Based on Phenological Phase Space and Temporal Profile Analysis. *Int. J. Environ. Res. Public Health* **2019**, *16*, 350. [CrossRef]
- 135. Zhang, Z.; Liu, M.; Liu, X.; Zhou, G. A New Vegetation Index Based on Multitemporal Sentinel-2 Images for Discriminating Heavy Metal Stress Levels in Rice. *Sensors* **2018**, *18*, 2172. [CrossRef]
- 136. Liu, T.; Liu, X.; Liu, M.; Wu, L. Evaluating Heavy Metal Stress Levels in Rice Based on Remote Sensing Phenology. *Sensors* **2018**, 18, 860. [CrossRef]
- 137. Zhang, C.; Ren, H.; Huang, Z.; Li, J.; Qin, Q.; Zhang, T.; Sun, Y. Assessment of the application of copper stress vegetation index on Hyperion image in Dexing Copper Mine, China. *J. Appl. Remote Sens.* **2019**, *13*, 014511. [CrossRef]
- 138. Liu, M.; Wang, T.; Skidmore, A.K.; Liu, X.; Li, M. Identifying rice stress on a regional scale from multi-temporal satellite images using a Bayesian method. *Environ. Pollut.* **2019**, 247, 488–498. [CrossRef]
- 139. Tang, Y.; Liu, M.; Liu, X.; Wu, L.; Zhao, B.; Wu, C. Spatio-temporal Index Based on Time Series of Leaf Area Index for Identifying Heavy Metal Stress in Rice under Complex Stressors. *Int. J. Environ. Res. Public Health* **2020**, *17*, 2265. [CrossRef]
- 140. Ma, B.; Yang, X.; Yu, Y.; Shu, Y.; Che, D. Investigation of Vegetation Changes in Different Mining Areas in Liaoning Province, China, Using Multisource Remote Sensing Data. *Remote Sens.* **2021**, *13*, 5168. [CrossRef]
- 141. Zhang, Y.; Liu, M.; Kong, L.; Peng, T.; Xie, D.; Zhang, L.; Tian, L.; Zou, X. Temporal Characteristics of Stress Signals Using GRU Algorithm for Heavy Metal Detection in Rice Based on Sentinel-2 Images. *Int. J. Environ. Res. Public Health* **2022**, 19, 2567. [CrossRef] [PubMed]
- 142. Kayet, N.; Pathak, K.; Singh, C.P.; Bhattacharya, B.K.; Kumar Chaturvedi, R.; Brahmandam, A.S.V.; Mandal, C. Detection and mapping of vegetation stress using AVIRIS-NG hyperspectral imagery in coal mining sites. *Adv. Space Res.* **2024**, *73*, 1368–1378. [CrossRef]
- 143. Qu, Y.H.; Jiao, S.H.; Liu, S.H.; Zhu, Y.Q. Retrieval of Copper Pollution Information from Hyperspectral Satellite Data in a Vegetation Cover Mining Area. *Spectrosc. Spectr. Anal.* **2015**, 35, 3176–3181.
- 144. Yang, X.; Lei, S.; Zhao, Y.; Cheng, W. Use of hyperspectral imagery to detect affected vegetation and heavy metal polluted areas: A coal mining area, China. *Geocarto Int.* **2022**, *37*, 2893–2912. [CrossRef]
- 145. Zhong, L.; Chu, X.; Qian, J.; Li, J.; Sun, Z. Multi-Scale Stereoscopic Hyperspectral Remote Sensing Estimation of Heavy Metal Contamination in Wheat Soil over a Large Area of Farmland. *Agronomy* **2023**, *13*, 2396. [CrossRef]
- 146. Khalili, R.; Anvari, S.; Honarmand, M. Combination of Biochemical and Hyperspectral Remote Sensing Methods for Detection of Heavy Metal Pollutions in Eucalyptus Leaves (Case Study: The City of Bam). *Int. Arch. Photogramm. Remote Sens. Spat. Inf. Sci.* **2015**, XL-1/W5, 379–385. [CrossRef]
- 147. Hede, A.N.H.; Kashiwaya, K.; Koike, K.; Sakurai, S. A new vegetation index for detecting vegetation anomalies due to mineral deposits with application to a tropical forest area. *Remote Sens. Environ.* **2015**, *171*, 83–97. [CrossRef]
- 148. Jin, M.; Liu, X.; Zhang, B. Evaluating Heavy-Metal Stress Levels in Rice Using a Theoretical Model of Canopy-Air Temperature and Leaf Area Index Based on Remote Sensing. *IEEE J. Sel. Top. Appl. Earth Obs. Remote Sens.* 2017, 10, 3232–3242. [CrossRef]
- 149. Wu, C.; Liu, M.; Liu, X.; Wang, T.; Wang, L. Developing a New Spectral Index for Detecting Cadmium-Induced Stress in Rice on a Regional Scale. *Int. J. Environ. Res. Public Health* **2019**, *16*, 4811. [CrossRef] [PubMed]
- 150. Li, X.; Li, L.; Liu, X. Collaborative inversion heavy metal stress in rice by using two-dimensional spectral feature space based on HJ-1 A HSI and radarsat-2 SAR remote sensing data. *Int. J. Appl. Earth Obs. Geoinf.* **2019**, *78*, 39–52. [CrossRef]
- 151. Li, Y.; Yang, K.; Zhao, H. Scale transfer learning of hyperspectral prediction model of heavy metal content in maize: From laboratory to satellite. *Int. J. Remote Sens.* **2023**, *44*, 2590–2610. [CrossRef]
- 152. Li, J.; Pei, Y.; Zhao, S.; Xiao, R.; Sang, X.; Zhang, C. A Review of Remote Sensing for Environmental Monitoring in China. *Remote Sens.* **2020**, *12*, 1130. [CrossRef]

Remote Sens. **2024**, 16, 3221 30 of 30

153. Gorelick, N.; Hancher, M.; Dixon, M.; Ilyushchenko, S.; Thau, D.; Moore, R. Google Earth Engine: Planetary-scale geospatial analysis for everyone. *Remote Sens. Environ.* **2017**, 202, 18–27. [CrossRef]

- 154. Li, J.; Humphrey, M.; Van Ingen, C.; Agarwal, D.; Jackson, K.; Ryu, Y. eScience in the cloud: A modis satellite data reprojection and reduction pipeline in the windows azure platform. In Proceedings of the 2010 IEEE International Symposium on Parallel and Distributed Processing (IPDPS), Atlanta, GA, USA, 19–23 April 2010; pp. 1–10.
- 155. Storch, T.; Reck, C.; Holzwarth, S.; Wiegers, B.; Mandery, N.; Raape, U.; Strobl, C.; Volkmann, R.; Böttcher, M.; Hirner, A.; et al. Insights into CODE-DE—Germany's Copernicus data and exploitation platform. *Big Earth Data* **2019**, *3*, 338–361. [CrossRef]
- 156. Apicella, L.; De Martino, M.; Quarati, A. Copernicus User Uptake: From Data to Applications. *ISPRS Int. J. Geo-Inf.* **2022**, *11*, 121. [CrossRef]
- 157. Dehghan-Shoar, M.H.; Orsi, A.A.; Pullanagari, R.R.; Yule, I.J. A hybrid model to predict nitrogen concentration in heterogeneous grassland using field spectroscopy. *Remote Sens. Environ.* **2023**, *285*, 113385. [CrossRef]
- 158. Fotovat, A.; Naidu, R.; Sumner, M.E. Water: Soil ratio influences aqueous phase chemistry of indigenous copper and zinc in soils. *Soil Res.* **1997**, *35*, 687–710. [CrossRef]
- 159. Hassanpour, R.; Zarehaghi, D.; Neyshabouri, M.R.; Feizizadeh, B.; Rahmati, M. Modification on optical trapezoid model for accurate estimation of soil moisture content in a maize growing field. *J. Appl. Remote Sens.* **2020**, *14*, 034519. [CrossRef]
- 160. Rahmati, M.; Hamzehpour, N. Quantitative remote sensing of soil electrical conductivity using ETM+ and ground measured data. *Int. J. Remote Sens.* **2017**, *38*, 123–140. [CrossRef]
- 161. Rahmati, M.; Oskouei, M.; Neyshabouri, M.; Walker, J.; Fakherifard, A.; Ahmadi, A.; Mousavi, S. Soil moisture derivation using triangle method in the lighvan watershed, north western Iran. *J. Soil Sci. Plant Nutr.* **2015**, *15*, 167–178. [CrossRef]
- 162. Kabata-Pendias, A. Trace Elements in Soils and Plants; CRC Press: Boca Raton, FL, USA, 2010; p. 548.
- 163. Jonard, F.; De Cannière, S.; Brüggemann, N.; Gentine, P.; Short Gianotti, D.J.; Lobet, G.; Miralles, D.G.; Montzka, C.; Pagán, B.R.; Rascher, U.; et al. Value of sun-induced chlorophyll fluorescence for quantifying hydrological states and fluxes: Current status and challenges. *Agric. For. Meteorol.* **2020**, *291*, 108088. [CrossRef]
- 164. Drusch, M.; Moreno, J.; Del Bello, U.; Franco, R.; Goulas, Y.; Huth, A.; Kraft, S.; Middleton, E.M.; Miglietta, F.; Mohammed, G.; et al. The FLuorescence EXplorer Mission Concept—ESA's Earth Explorer 8. *IEEE Trans. Geosci. Remote Sens.* 2017, 55, 1273–1284. [CrossRef]
- 165. Rathod, P.H.; Müller, I.; Van der Meer, F.D.; de Smeth, B. Analysis of visible and near infrared spectral reflectance for assessing metals in soil. *Environ. Monit. Assess.* **2016**, *188*, 558. [CrossRef]
- 166. Wei, L.; Yuan, Z.; Zhong, Y.; Yang, L.; Hu, X.; Zhang, Y. An Improved Gradient Boosting Regression Tree Estimation Model for Soil Heavy Metal (Arsenic) Pollution Monitoring Using Hyperspectral Remote Sensing. *Appl. Sci.* **2019**, *9*, 1943. [CrossRef]
- 167. Hong, Y.; Shen, R.; Chen, S.; Chen, Y.; Guo, L.; He, J.; Liu, Y.; Yu, L.; Liu, Y. Cadmium concentration estimation in peri-urban agricultural soils: Using reflectance spectroscopy, soil auxiliary information, or a combination of both? *Geoderma* **2019**, 354, 113875. [CrossRef]
- 168. Zhang, X.; Sun, W.; Cen, Y.; Zhang, L.; Wang, N. Predicting cadmium concentration in soils using laboratory and field reflectance spectroscopy. *Sci. Total Environ.* **2019**, *650*, 321–334. [CrossRef]
- 169. Han, A.; Lu, X.; Qing, S.; Bao, Y.; Bao, Y.; Ma, Q.; Liu, X.; Zhang, J. Rapid Determination of Low Heavy Metal Concentrations in Grassland Soils around Mining Using Vis–NIR Spectroscopy: A Case Study of Inner Mongolia, China. *Sensors* **2021**, *21*, 3220. [CrossRef]
- 170. Yousefi, G.; Homaee, M.; Norouzi, A.A. Estimating soil heavy metals concentration at large scale using visible and near-infrared reflectance spectroscopy. *Environ. Monit. Assess.* **2018**, *190*, 513. [CrossRef]
- 171. Zhao, L.; Hu, Y.M.; Zhou, W.; Liu, Z.H.; Pan, Y.C.; Shi, Z.; Wang, L.; Wang, G.X. Estimation Methods for Soil Mercury Content Using Hyperspectral Remote Sensing. *Sustainability* **2018**, *10*, 2474. [CrossRef]
- 172. Sun, W.; Zhang, X.; Sun, X.; Sun, Y.; Cen, Y. Predicting nickel concentration in soil using reflectance spectroscopy associated with organic matter and clay minerals. *Geoderma* **2018**, 327, 25–35. [CrossRef]
- 173. Song, T.; Fu, X.; Chen, Y.; Wei, Y.; Wang, Q.; Cheng, X. Remote Sensing Inversion of Soil Zinc Pollution in Gejiu Mining Area of Yunnan. *Remote Sens. Technol. Appl.* **2018**, 33, 88–95.
- 174. Sun, W.; Zhang, X. Estimating soil zinc concentrations using reflectance spectroscopy. *Int. J. Appl. Earth Obs. Geoinf.* **2017**, 58, 126–133. [CrossRef]
- 175. Liu, M.; Skidmore, A.K.; Wang, T.; Liu, X.; Wu, L.; Tian, L. An approach for heavy metal pollution detected from spatio-temporal stability of stress in rice using satellite images. *Int. J. Appl. Earth Obs. Geoinf.* **2019**, *80*, 230–239. [CrossRef]
- 176. Zhang, B.; Liu, X.; Liu, M.; Meng, Y. Detection of Rice Phenological Variations under Heavy Metal Stress by Means of Blended Landsat and MODIS Image Time Series. *Remote Sens.* **2019**, *11*, 13. [CrossRef]

**Disclaimer/Publisher's Note:** The statements, opinions and data contained in all publications are solely those of the individual author(s) and contributor(s) and not of MDPI and/or the editor(s). MDPI and/or the editor(s) disclaim responsibility for any injury to people or property resulting from any ideas, methods, instructions or products referred to in the content.